CURATION LEAKS: MEMBERSHIP INFERENCE ATTACKS AGAINST DATA CURATION FOR MACHINE LEARNING

Anonymous authors
Paper under double-blind review

ABSTRACT

In machine learning, data curation is used to select the most valuable data for improving both model accuracy and computational efficiency. Recently, curation has also been explored as a solution for private machine learning: rather than training directly on sensitive data, which is known to leak information through model predictions, the private data is used only to guide the selection of useful public data. The resulting model is then trained solely on curated public data. It is tempting to assume that such a model is privacy-preserving because it has never seen the private data. Yet, we show that without further protection curation pipelines can still leak private information. Specifically, we introduce novel attacks against popular curation methods, targeting every major step: the computation of curation scores, the selection of the curated subset, and the final trained model. We demonstrate that each stage reveals information about the private dataset, and that even models trained exclusively on curated public data leak membership information about the private data that guided curation. These findings highlight the inherent privacy risks in data curation that were previously overlooked, and suggest that (1) in the context of curation, privacy analysis must extend beyond the training procedure to include the data selection process, and (2) true privacy-preserving curation will require new methods with formal privacy guarantees.

1 INTRODUCTION

Data curation has become an important part of modern machine learning (ML) pipelines (Maini et al., 2024; Wu et al., 2024), offering a principled way to select high-value data in order to maximize model performance and computational efficiency. By filtering out noisy, low-quality, or redundant samples (Gadre et al., 2023; Li et al., 2024a; Gu et al., 2025; Thrush et al., 2025), curation allows to train on the most informative points, thus improving generalization and resource utilization.

This paradigm is also particularly appealing for sensitive domains, such as finance or healthcare, where the available training datasets are usually limited, which hinders the training of powerful ML models. In these settings, curation offers a key advantage: it enables model developers to leverage publicly available data pools and select a subset from these that is most relevant to their target application. Typically, the small in-domain target dataset, which represents the actual distribution of interest, or the downstream data the model is expected to perform well on, is used to guide this selection. Various techniques have been proposed to perform such guidance: for example, identifying public samples that are most similar to the target data in feature space (Gadre et al., 2023; Yu et al., 2024), scoring public samples based on how much they improve accuracy on the target set (Thrush et al., 2025), or maximizing a data attribution or influence metric (Park et al., 2023; Engstrom et al., 2024). The curated public dataset is finally used to train an ML model that outperforms models trained on *all* public data or achieves similar results with greater computational efficiency on target domain tasks. Importantly, the resulting model is never directly exposed to the target dataset.

Due to these advantages, curation is widely used in practice. Curated datasets are routinely released to the public (Penedo et al., 2023; Li et al., 2024b; Penedo et al., 2024), and in some cases, even the intermediate quality scores are made available (Computer, 2023). Furthermore, there exists a growing market of data curation as a service, where datasets, scores, and subsets are exchanged between organizations (DatalogyAI; Snorkel; ScaleAI) Yet, the privacy risks for the target data under such practices are, to date, not well understood. Therefore, in this paper, we provide the first systematic study of privacy risks in curation pipelines. Therefore, we carry out custom membership inference attacks (Shokri et al., 2017; Carlini et al., 2022a) on data points from the target set at every stage of the pipeline, and demonstrate that each step can leak private information.

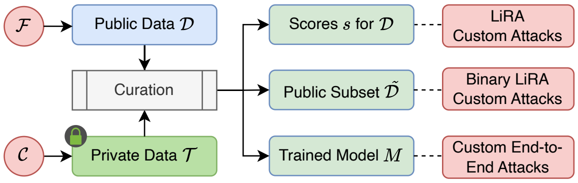
$\mathcal{F}$
Public Data $\mathcal{D}$
Curation
$\mathcal{C}$
Private Data $\mathcal{T}$
Scores s for $\mathcal{D}$
LiRA Custom Attacks
Public Subset $\tilde{\mathcal{D}}$
Binary LiRA Custom Attacks
Trained Model M
Custom End-to-End Attacks

Figure 1: **We attack private data $\mathcal{T}$ used to curate a public dataset $\mathcal{D}$.** We show that the scores s, top-scoring subsets $\tilde{\mathcal{D}}$ and even trained models M leak membership information.

Concretely, we design and evaluate attacks against 1) the curation methods' released scores, 2) the selected public subsets, and 3) the final trained model, as shown in Figure 1. To attack curation scores, we employ Likelihood Ratio Attack (LiRA) (Carlini et al., 2022a) and a custom attack based on a voting scheme. We show that image embedding-based curation that relies on a nearest-neighbor mechanism creates high vulnerability for samples with non-zero influence, while TRAK's averaging provides better protection but remains vulnerable for small datasets. To attack the curated public subset, we adapt LiRA to the binary setting, where the adversary only knows if a sample was picked by the curation or not. Additionally, we design a custom attack that iteratively performs the membership inference using the deterministic behaviour of the curation mechanism. Finally, to attack the trained model, we insert samples $\mathcal{F}$ into the pool whose curation score is highly influenced by a particular target, and which imprint a measurable signal in the model if trained on. The addition of such samples represents a realistic setup where the public pool data is often scraped from the internet and prior work has shown that it is possible to introduce targetly manipulated data points into ML model training pipelines this way (Carlini et al., 2024). Because our attacks succeed with only a small number of inserted samples, they hold the potential to pose a risk in real-world curation settings where public data is reused. Overall, our findings highlight that curation-guided approaches can still leak privacy, and that careful analysis and new safeguards are needed to ensure robust data protection.

To summarize, we make the following main contributions:

1. We present the first comprehensive privacy analysis of data curation pipelines, highlighting that curation leaks private information at each step: the scores, curation sets, and the final model.
2. We design custom membership attacks for each curation step, showing that both curation scores and curated datasets leak membership information without pipeline modifications.
3. We show that even end-to-end attacks on the final model can leak target data information by inserting only a small number of crafted samples into public datasets.
4. Our empirical evaluation on six datasets and two curation methods shows that, while TRAK is more robust than image-based curation, it remains highly vulnerable for small datasets, the very scenario motivating curation in sensitive domains.

2 Background and Related Work

Data Attribution. The influence of training samples on the behaviour of a trained ML model on some target data point is determined via data attribution methods. The *DataModels* approach (Ilyas et al., 2022) trains many models on different training data subsets and then fits an influence estimator. TRAK (Park et al., 2023) peforms data attribution using closed-form influence functions for Logistic Regression. To make that applicable to deep learning, they formulate the model training as a logistic regression on gradients of a trained model. With that approach, TRAK is more efficient than DataModels, but still requires training in the order of ~ 20 models and another backward pass for each on the full training set. Ilyas & Engstrom (2025) introduce an alternative which requires training just one model, but requires a full backward pass on the entire training dataset for each target sample. By selecting those training samples with the highest positive attribution scores, data attribution methods can serve as methods for data curation (Engstrom et al., 2024).

Data Curation. The goal of data curation is to select the most valuable data for training. Gadre et al. (2023) introduce *DataComp*, an ML challenge of obtaining the highest accuracy just by modifying the training data. They also developed image-based filtering for selecting appropriate images based on semantic similarity. Thrush et al. (2025) propose attributing training data performance to target utility by computing correlations on the loss of the training data and the target utility. Notably, this allows computing correlations for data that the models have not been trained on, sparing the computationally expensive setup that *e.g.,* TRAK- or DataModels-based curation requires.

In this work, we focus on two representative curation methods, namely image embedding-based curation (Gadre et al., 2023) and TRAK (Park et al., 2023). In both cases, we have a public dataset $\mathcal{D} = \{x_i\}_{i=1}^{N}$ and a private dataset $\mathcal{T} = \{t_i\}_{i=1}^{n}$. We call *curating* $\mathcal{D}$ *for* $\mathcal{T}$ when we try to obtain a subset $\tilde{\mathcal{D}} \subseteq \mathcal{D}$ s.t. the performance and/or compute efficieny for utility on $\mathcal{T}$ is improved by training on $\tilde{\mathcal{D}}$ instead of the full $\mathcal{D}$.

Image Embedding-based Curation. Image embedding-based curation assigns scores based on the cosine similarity of image-embeddings. For each image x_i in the public curation pool $\mathcal{D}$, the score is the maximum similarity to a sample t_j in the private target set $\mathcal{T}$, *i.e.,* $s(x_i) = \max_{j \in n} \cos(\phi(x_i), \phi(t_j))$ where $\phi(\cdot)$ is the embedding function.

TRAK. TRAK computes attribution scores via projected gradients to identify influential pool samples. Following Engstrom et al. (2024), in this work, we compute our scores as the *average attribution score* on $\mathcal{T}$, *i.e.,* $s(x_i) = \frac{1}{n} \sum_j^n \Phi_i^T G_j$ where $G_\mathcal{T}$ are the gradients of $\mathcal{T}$. Φ are the TRAK features. We obtain them from the gradients X of $\mathcal{D}$ as $\Phi = X(X^T X)^{-1} Q$. Q are the scaling factors, determined as the gradient of model output to loss.

Assessing Privacy Risks in ML. The de facto standard for assessing the privacy risks in ML systems is to rely on Membership Inference Attacks (MIAs) (Shokri et al., 2017; Carlini et al., 2022a). A popular attack to perform membership inference is LiRA (Carlini et al., 2022a), which we build upon in this work to asses the privacy risks in data curation pipelines. It trains *shadow models* on various subsets of the target data and then fits distributions to the observed behaviour of the models with a target vs. those without a target. Then, to attack a model, it compares the likelihoods of the observed behaviour under the distribution of the target being in the training vs. being not in the training data. The ratio of these likelihoods serves as the membership score. In this work, we rely on adaptions of LiRA, but instead of training shadow models, we perform curation on random subsets of the target data to obtain *shadow sets*, *i.e.,* the curation results for the random subsets. We then select high-signal measurements similar to Jagielski et al. (2023), *i.e.,* those that differ most significantly for a specific target, and compute the membership inference scores as the log-likelihood ratios.

3 Attacking Data Curation Pipelines

In this section, we explore privacy leakage from the different stages of data curation pipelines outlined in Figure 1. We start off by outlining the threat model and adversary goal and capabilities in Section 3.1. Then, we attack three progressively harder threat models: (1) continuous curation scores (Section 3.2), (2) binary selection masks (Section 3.3), and (3) final trained models (Section 3.4). Finally, we summarize our attacks in Section 3.5.

3.1 Threat Model

Adversary Goal. Our attacks infer membership in the *private target set* $\mathcal{T}_{\text{sel}} \subseteq \mathcal{T}$ used for curation, *i.e.,* for a given target t whether $t \in \mathcal{T}_{\text{Sel.}}$. A target sample t can influence the curation scores s, and through that, subsequently, the curated public dataset $\tilde{\mathcal{D}}$ and, finally, the model $\mathcal{M}$ trained on $\tilde{\mathcal{D}}$. Unlike in classical MIA (Shokri et al., 2017; Carlini et al., 2022a) t is never part of the training data of the model $\mathcal{M}$ directly, *i.e.,* $\tilde{\mathcal{D}} \cap \mathcal{T} = \emptyset$.

Adversary Capabilities and Knowledge. Across all pipeline stages, we assume the following **adversary knowledge**; (1) The full public pool $\mathcal{D}$. Since such pools are often web-scale dataset from the internet, we assume the adversary can obtain it as well. (2) The target dataset $\mathcal{T}$. This follows standard assumptions in MIAs (Shokri et al., 2017) where the adversary knows the target samples whose membership they want to infer. (3) The curation algorithm used (*e.g.,* Image-based or TRAK). Curation methods are often open-source or disclosed in model documentation. For **adversary capabilities** we assume the adversary can observe only the outcome of the respective curation stage, *i.e.,* the scores s or the selection mask m or (through black-box query access) the

Attack Surface	**Goal**	**Knowledge**	**Capabilities**	**Observations**
Scores (Section 3.2)	Infer $\mathcal{T}_{\text{Sel.}} \subseteq \mathcal{T}$	Public pool $\mathcal{D}$, target set $\mathcal{T}$, curation algorithm	Passive observation	Scores $s \in \mathbb{R}^{\|\mathcal{D}\|}$
Subset (Section 3.3)			Passive observation	Selection $m \in \{0,1\}^{\|\mathcal{D}\|}$
Final Model (Section 3.4)			**Inject** fingerprinted samples $\mathcal{F}$ into $\mathcal{D}$ before curation	Trained model $\mathcal{M}$ (black-box query access)

Table 1: **Threat model summary.** All adversaries aim to infer membership in the private curation target set $\mathcal{T}_{\text{sel}}$ (*not* training-set membership). Scores provide fine-grained ranking information, subsets reveal only binary selection, and final models require active poisoning with detectable fingerprints.

trained model $\mathcal{M}$. Only for the attacks on the final models we assume that a small part of the public pool can be poisoned, as Carlini et al. (2024) have shown to be realistic. Table 1 summarizes this.

3.2 Score-Based Attacks

Adapting LiRA. To assess privacy leakage from curation scores, we adapt LiRA (Carlini et al., 2022a) for curation setups. Concretely, we sample m different random subsets from the target dataset $\mathcal{T}$ and perform curation based on each of them. Each target is in exactly half of the random subsets, ensuring an unbiased estimate of the in/out distributions. The resulting *shadow sets* $\{s_i \in \mathbb{R}^N\}_{j=1}^m$ with $N = |\mathcal{D}|$ of curation scores take the role of the shadow models in the original LiRA (see Appendix B.1 for details). For each shadow set, we have the ground truth information on which of the data points from the target dataset was a member. With $N \approx$ 12.8M pool samples, most measurements are noise. Following Jagielski et al. (2023), we select only the single most informative public sample per target:

$$k^* = \arg\max_{k \in [N]} \left| \mathbb{E}_{j:t \in \mathcal{T}_j}[s_j^{(k)}] - \mathbb{E}_{j:t \notin \mathcal{T}_j}[s_j^{(k)}] \right|. \tag{1}$$

Custom Voting (Image-based). Image-based curation's deterministic nearest-neighbor structure ($s(x) = \max_t \cos(\phi(x), \phi(t))$) enables reverse-engineering: for each public sample, identify which target $t^* = \arg\min_t |s(x) - \text{sim}(\phi(x), \phi(t))|$ was responsible, increment $v_{\text{vote}}(t^*)$ (positive evidence), and decrement votes for all t where $\text{sim}(\phi(x), \phi(t)) > s(x)$ (negative evidence—if t were present, $s(x)$ would be higher).

Least Squares (TRAK). TRAK-based curation computes scores as $s(x) = \frac{1}{|\mathcal{T}|} \sum_t \Phi(x)^\top G_t$. We can reformulate membership inference as a linear problem. We denote $m \in \{0, 1/|\mathcal{T}|\}^{|\mathcal{T}|}$ the masked mean operator. To recover membership signals, we then solve

$$\underset{m \in \mathbb{R}^n}{\text{minimize}} \quad \|\Phi(x)^\top G_t m - s\|_2^2. \tag{2}$$

The membership scores are then the optimal weights $v_{\text{lstsq}} = m$. We further detail this in Appendix B.4.2. Over both curation method, the **final LiRA membership inference score** for each target sample is then computed as

$$v_{\text{LiRA}}(t) = \log\left(p(s_{k^*(t)} | \mathcal{N}\left(\mu_{in}, \sigma_{in}^2\right))\right) - \log\left(p(s_{k^*(t)} | \mathcal{N}\left(\mu_{out}, \sigma_{out}^2\right))\right), \tag{3}$$

where $s_{k^*(t)}$ is the score of the public sample we identified as described above. For **Image-based Curation** the voting-based attack scores are the number votes v_{vote}. We empirically compare both attacks and find our custom attack outperforms LiRA.

3.3 Subset Selection Attacks

Assessing the privacy risks of the curated public subset is significantly more challenging than attacking the curation scores. This is because the scores yield a fine-grained ranking of the public samples whereas the curated dataset itself can be considered as a binary mask that only indicates for each public data point in the pool $\mathcal{D}$ whether it was included into the curated set $\tilde{\mathcal{D}}$.

Once again, we adapt LiRA. While the original LiRA is designed to operate on continuous output logits, we need our attack to operate on *binary* selection observations. In line with the setup presented in the previous section, we again sample m different random subsets from the target dataset $\mathcal{T}$ to obtain our *shadow sets* $\{s_i \in \mathbb{R}^N\}_{j=1}^m$ which we binarize to top-k masks$\{\bar{s}_i \in \{0,1\}^N\}_{j=1}^m$ to represent which samples from the public pool were chosen by the curation.

In a naïve setup, we directly model these binary shadow set outcomes using Bernoulli distributions. For each $t \in \mathcal{T}$ we compute $\mu_{in} \in \mathbb{R}^N$ as the average of s_i for every $t \in \mathcal{T}_i$ and $\mu_{out} \in \mathbb{R}^N$ where $t \notin \mathcal{T}_i$. These are the frequencies of public samples being in the top set depending on whether t was part of the curation target. We again filter for each target t the pool sample x_t that is most indicative of t's presence, *i.e.,* shows the highest difference between $\mu_{\text{in},t}$ and $\mu_{\text{out},t}$. When computing the membership inference scores for the private subset, we only look at whether x_t is present or not and compute the membership score as the log-likelihood ratio for the Bernoulli distribution

$$v_{\text{Binary LiRA}}(t) \log\left(\frac{P(x_v \mid \mu_{\text{in},t})}{P(x_v \mid \mu_{\text{out},t})}\right) = \log\left(\frac{\mu_{\text{in},t}^{x_v}(1-\mu_{\text{in},t})^{1-x_v}}{\mu_{\text{out},t}^{x_v}(1-\mu_{\text{out},t})^{1-x_v}}\right). \tag{4}$$

Soft Binarization. Shadow sets contain continuous scores before binarization. Rather than discarding this, we apply sigmoid transformation $\tilde{s} = \sigma_{\pi_k}(s_i) = 1/(1+\exp(-\gamma \cdot (s_i - \pi_k)/\tau))$ to preserve boundary proximity information. This helps when samples cluster near threshold (CIFAR-10) but not when clearly separated (RESISC45).

Iterative Membership Inference Attack (Image-based). We use curation as an oracle during the attack: given hypothesis $\tilde{\mathcal{T}}_i$, we curate the public pool $\mathcal{D}$ and compare our result $\tilde{\mathcal{D}}_i$ with $\tilde{\mathcal{D}}$. Overweighted samples (*i.e.,* $x \in \tilde{\mathcal{D}}_i$ but $x \notin \tilde{\mathcal{D}}$) suggest wrong targets; underweighted samples (*i.e.,* $x \in \tilde{\mathcal{D}}$ but $x \notin \tilde{\mathcal{D}}_i$) suggest missing targets. We iteratively refine the hypothesis $\tilde{\mathcal{T}}_i$ until convergence.

Voting-based Membership Inference Initialize $\tilde{\mathcal{T}}_0 = \{\emptyset\}$ and a vote accumulator $v_{\text{Iterative}}(t) = 0$ for each $t \in \mathcal{T}$. At iteration i:

$$\tilde{\mathcal{D}}_i = \text{Curate}(\mathcal{D}, \tilde{\mathcal{T}}_i) \tag{5}$$

$$\mathcal{O}_i = \{x \in \tilde{\mathcal{D}}_i : x \notin \tilde{\mathcal{D}}\} \quad \text{(overweighted samples)} \tag{6}$$

$$\mathcal{U}_i = \{x \in \tilde{\mathcal{D}} : x \notin \tilde{\mathcal{D}}_i\} \quad \text{(underweighted samples)} \tag{7}$$

Update votes for each target $t \in \tilde{\mathcal{T}}_i$:

$$v_{\text{Iterative}}(t) \leftarrow v_{\text{Iterative}}(t) - \mathbb{1}[t = \arg\max_{t' \in \tilde{\mathcal{T}}_i} \text{sim}(\phi(x), \phi(t'))], \quad \forall x \in \mathcal{O}_i \tag{8}$$

$$v_{\text{Iterative}}(t) \leftarrow v_{\text{Iterative}}(t) + \mathbb{1}[t = \arg\max_{t' \in \tilde{\mathcal{T}}_i} \text{sim}(\phi(x), \phi(t'))], \quad \forall x \in \mathcal{U}_i \tag{9}$$

Keep targets with a positive sum of votes

$$\tilde{\mathcal{T}}_{i+1} = \{t \in \tilde{\mathcal{T}}_i : v_{\text{Iterative}}(t) \geq 0\}. \tag{10}$$

Iterate until $J(\tilde{\mathcal{D}}_i, \tilde{\mathcal{D}}) \geq \theta$ or early stopping criteria are met, where $J(\cdot,\cdot)$ denotes Jaccard similarity.

The process converges when it finds a set $\tilde{\mathcal{T}}_i$ producing a selection pattern matching the target's, though multiple solutions may exist due to the many-to-one mapping between targets and selected samples. The votes $v_{\text{Iterative}}(t_i)$ for each target $t_i \in \tilde{\mathcal{T}}_i$ are then the membership inference scores

For **TRAK-based Curation**, we use the original membership scores output by LiRA directly. We therefore have membership inference scores $v_{\text{Binary LiRA}}$ from the binarized LiRA, $v_{\text{Sig Binary LiRA}}$ from binarized LiRA fitted with smoothed shadow sets and the iteratively computed votes $v_{\text{Iterative}}$ from the custom attack. We empirically compare these attacks.

3.4 Final Models Attack

Finally, we assess privacy leakage of the target data from the final model $\mathcal{M}$ trained purely on the curated public data. This represents the highest threat as such end-to-end attack could actually be instantiated against exposed models that are trained based on curated data.

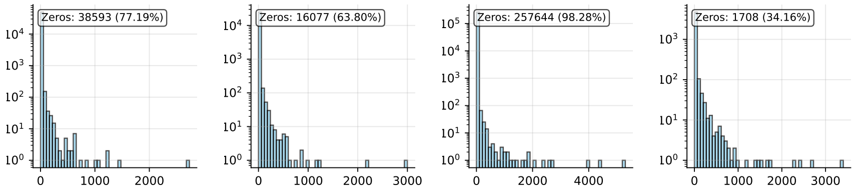

(a) CIFAR-10 (b) RESISC45 (c) PCAM (d) STL10

Figure 2: **Influence sparsity in Image-based curation.** Distribution of how many public samples have each target as their nearest neighbor. The concentration at zero demonstrates that most targets have no direct influence on curation scores, necessitating our fingerprinting approach.

To successfully extract membership information in this end-to-end setup, we rely on inserting a few modified samples $\mathcal{F}$ into the large curation pool. This is a realistic setup, as shown by Carlini et al. (2024), who have shown various practical ways of putting adversarial examples into web-scale training data. Samples in $\mathcal{F}$ must satisfy two critical requirements:

1. **Selective triggering:** Each sample must be selected during curation if and only if a specific target $t \in \mathcal{T}$ is present in the private target set. This requires crafting samples whose curation scores are sensitive to individual targets rather than the aggregate properties of $\mathcal{T}$.
2. **Detectable fingerprint:** Selected samples must imprint a measurable signal, which we call a *fingerprint*, in the trained model $\mathcal{M}$ that the adversary can later detect to infer membership.

In **Image-Based Curation**, selection from the pool depends solely on image embeddings. Hence, we can modify text captions arbitrarily without affecting curation scores. Being able to arbitrarily modify captions has been shown sufficient for imprinting a measurable signal in trained models (Carlini & Terzis, 2022). However, achieving selective triggering remains challenging due to the sparse influence structure of nearest-neighbor selection. As illustrated in Figure 2, in the unmodified setup, most target samples have zero influence on public sample scores under nearest-neighbor curation. Specifically, 77.19% (CIFAR-10), 63.80% (RESISC45), and 98.28% (PCAM) of target samples are not the nearest neighbor for any public sample. This sparsity creates both a challenge (most targets are unattackable by default) and an opportunity (influenced samples have a strong membership signal).

To overcome influence sparsity, we inject fingerprinted samples $\mathcal{F}$ into the public pool. We construct candidates for candidates for $\mathcal{F}$ from images in $\mathcal{D}$ paired with semantically unrelated captions to the target data (*e.g.,* a fingerprint for CIFAR10 "ratatouille"). We find that including captions from the target dataset prevents the fingerprint from being detectable, as the final model will pick these captions more often over unrelated captions. For each candidate fingerprint f and target t_i, we compute a correspondence score balancing two objectives:

$$\text{score}(f, t_i) = \alpha \cdot \underbrace{\text{sim}(\phi(f), \phi(t_i))}_{\text{attraction to } t} + (1 - \alpha) \cdot \underbrace{\left(1 - \max_{t' \in \mathcal{T} \setminus \{t_i\}} \text{sim}(\phi(f), \phi(t'))\right)}_{\text{repulsion from other targets}} \tag{11}$$

where $\alpha \in [0, 1]$ trades off between proximity to the intended target and separation from samples in the target set. Our attack inserts as fingerprints $\mathcal{F} = \{\arg\max_{f \in \mathcal{D}} \text{score}(f, t_i) | t_i \in \mathcal{T}\}$, *i.e.,* the highest-scoring sample for each target. This mapping is not unique, so $|\mathcal{F}| \leq |\mathcal{T}|$.

Computationally Tractable End-to-End Attacks. Figure 10 in Appendix C.2 shows that including such a fingerprinted sample has a measurable effect on the final model. The results show that the fingerprint detection can be performed reliably: For a fixed number of 5 fingerprint samples, there is a constant signal for dataset sizes up to 1,000,000 (the maximum we evaluated), at which point the poisoning rate is 0.0005%. As training large models from scratch for every membership inference experiment is computationally intractable, we once establish the signal and from now on assume that the adversary can measure whether $f \in \tilde{\mathcal{D}}$. Therefore, we build our attacks on measurements of fingerprinted samples in $\tilde{\mathcal{D}}$.

We compute membership scores as follows. Let p_0^f denote the baseline percentile rank of fingerprinted sample f when scored against the full target set $\mathcal{T}$. The adversary does not know the selection

Algorithm 1 TRAK Membership Inference via Fingerprint Detection

```
Require: Pool data $X$, target gradients $Y$, fingerprints $\mathcal{F}$, threshold assumption $\rho$
Ensure: Membership scores for each target
$G_\lambda^{-1} \leftarrow (X^\top X + \lambda I)^{-1}$                         ▷ Cholesky decomposition
$\mu \leftarrow \mathbb{E}[Y]$, $\Sigma \leftarrow \mathrm{Cov}[Y]$                                  ▷ Target statistics
$S \leftarrow \mathcal{F} G_\lambda^{-1} Y^\top$                                           ▷ Signal matrix
$\nu_i \leftarrow \sqrt{f_i^\top G_\lambda^{-1} \Sigma G_\lambda^{-1} f_i}$ for all $i$                        ▷ Noise scales
Initialize $\text{score}_j \leftarrow 0$ for all targets
for each target $j \in [n]$ do
    $i^*(j) \leftarrow \arg\max_i |S_{ij}|/\nu_i$                              ▷ Best fingerprint
    Compute $z_{H_0}, z_{H_1}$ via Sherman-Morrison
    $p_{H_0}, p_{H_1} \leftarrow$ percentile ranks of $z_{H_0}, z_{H_1}$
    $\text{confidence}_j \leftarrow |\text{clip}(p_{H_1}, \rho, 100) - \text{clip}(p_{H_0}, \rho, 100)|$
end for
for each observed fingerprint $f_i \in \tilde{\mathcal{D}}$ do
    for each target $j$ where $i^*(j) = i$ do
        if $p_{H_1} > \rho \wedge p_{H_0} \le \rho$ then                  ▷ Fingerprint crosses threshold
            $\text{score}_j \leftarrow \text{score}_j + \text{confidence}_j$
        end if
    end for
end for
return $\{\text{score}_j\}_{j=1}^n$
```

threshold τ but can conservatively assume they will pick from the top 50% of the pool. We model the probability of selecting f without its corresponding target as:

$$P_0(f) = \frac{1}{1 + \exp(-(p_0^f - \tau)/\sigma)}, \tag{12}$$

where σ controls the transition sharpness. For each fingerprinted sample we measure to be in $\tilde{\mathcal{D}}$ we set the membership inference score of the corresponding target(s)[1] to the *surprise* of the measurement of that sample under H_0 divided by the number of targets that share that fingerprint (see Algorithms 4 and 5 for details)

$$v_{\text{E2E Img.}}(t_i) = \frac{1[\text{ selected }] - P(\text{ selected } \mid P_0(f))}{n_{\text{sharing}}\,(f)}. \tag{13}$$

For **TRAK-based Curation**, we face the challenge that it relies on a gradient-based scoring mechanism. Unlike Image-based curation, TRAK explicitly penalizes mislabeled or semantically inconsistent samples through this gradient alignment scoring (Park et al., 2023), rendering our previous caption manipulation approach ineffective. However, we discover that TRAK scores remain stable when captions are augmented with semantically orthogonal information. Specifically, appending unrelated concepts to otherwise correct captions (*e.g.,* transforming "an image of an airplane" to "an image of an airplane and ratatouille") preserves high TRAK scores while enabling detectable model changes. As demonstrated in Figure 11, such augmented samples imprint measurable signals in the trained model despite minimal impact on curation scores. This phenomenon occurs because TRAK primarily evaluates gradient alignment along task-relevant dimensions. Orthogonal semantic additions contribute negligible projection onto these principal gradient directions, leaving scores largely unchanged while still influencing the final model through training.

We construct a candidate set $\mathcal{C} = \{c_1, \ldots, c_M\}$ that we will consider as fingerprints by copying target samples from $\mathcal{T}$ and augmenting their captions with orthogonal signals. For each candidate c_i and target y_j, we quantify the membership signal through the influence matrix S and, to account for interference from other targets, noise scales v_i:

$$S = \mathcal{C} G_\lambda^{-1} Y^\top \in \mathbb{R}^{M \times n}, \quad \nu_i = \sqrt{c_i^\top G_\lambda^{-1} \Sigma G_\lambda^{-1} c_i}, \tag{14}$$

[1] Target(s) in plural, as the mapping is not necessarily unique.

where $G_\lambda = X^\top X + \lambda I$ is the regularized Gram matrix of the public pool and Y contains target gradients. Entry S_{ij} measures how target t_j's inclusion affects fingerprint f_i's score. $\Sigma = \text{cov}(Y)$ captures target gradient variability. The signal-to-noise ratio $|S_{ij}|/\nu_i$ identifies fingerprints most sensitive to specific targets. We construct the final fingerprinting set $\mathcal{F} = \{\arg\max_i |S_{ij}|/\nu_i \mid j \in \{1, \ldots, n\}\}$,*i.e.,* with the highest SNR sample for each target.

For each fingerprint we compute its expected score under two hypotheses: H_0: Target j absent from victim's private set, H_1: Target j present in victim's private set. Using the Sherman-Morrison formula (Hager, 1989), which enables efficient rank-one updates to matrix inverses, we compute these scores and their percentile ranks relative to the public pool distribution. The membership evidence is quantified by the percentile shift:

$$\text{confidence}_j = |\text{percentile}_{H_1}(f_{i^*(j)}) - \text{percentile}_{H_0}(f_{i^*(j)})|. \tag{15}$$

Since the adversary cannot observe the percentiles during the attack but only the presence of fingerprinted samples, we ideally want samples that *cross the selection threshold* ρ if and only if the corresponding target is included. Since the adversary does not know ρ, we conservatively assume it to be 0.5, *i.e.,* that the training data will only be picked from the better half. Using this assumption, the percentiles are are clipped to $[50, 100]$, s.t. changes in the lower percentiles do not affect confidence.

The membership inference score for target t_j is determined by whether its corresponding fingerprint $f_{i^*(j)}$ appears in $\tilde{\mathcal{D}}$. If the fingerprint is selected when it would not have been without target t_j (crossing the selection threshold), we set the membership score to the confidence value confidence$_j$, which represents the strength of the membership signal, so

$$v_{\text{E2E Trak}}(t_j) = \begin{cases} \text{confidence}_j & \text{if } f_{i^*(j)} \in \tilde{\mathcal{D}} \\ 0 & \text{otherwise} \end{cases}. \tag{16}$$

Algorithm 1 provides the complete attack procedure.

3.5 Summary of Attacks

We developed **8 attacks** across the three pipeline stages. Our **Score-Based Attacks (Section 3.2)** infer membership information from the curation scores. The **(1) LiRA**-based attack adapts likelihood ratio tests by running shadow curation processes and comparing score distributions between member and non-member scenarios for both Image-based and TRAK-based methods. **(2) Voting Scheme** exploits Image-based curation by reverse-engineering nearest-neighbor relationships through voting across shadow model predictions. **(3) Least Squares** and **(4) Orthogonal Matching Pursuit** solve linear systems that relate TRAK-based curation scores to private dataset membership. Our **Subset Selection Attacks (Section 3.3)** target the binary selection decisions made by curation. **(5) Binary LiRA** adapts the likelihood ratio framework to binary subset selection by modeling selection probabilities as Bernoulli distributions and comparing likelihoods under member versus non-member hypotheses. **(6) Iterative Voting Scheme** iteratively refines a hypothesis of the target set by running curation on candidate sets and adjusting the hypothesis until the resulting selection matches that of the target set. Finally, our **End-to-End Model Attacks (Section 3.4)** exploit the downstream model trained on curated data. **(7) Fingerprinting (Image-based)** uses mislabeled captions as fingerprints, selecting them via correspondence scoring to ensure they appear only when specific private examples are present in curation. **(8) Fingerprinting (TRAK)** employs benign captions with added orthogonal information as fingerprints, selecting them based on signal-to-noise ratio and threshold crossing detection to maximize their differential presence across shadow scenarios.

4 Evaluation

Experimental Setup. We evaluate our attacks using CommonPool (small) (Gadre et al., 2023) as the public dataset $\mathcal{D}$, containing 12.8M samples. We evaluate across six diverse target datasets spanning natural images, medical imaging, and satellite imagery to cover a wide range of curation setups: CIFAR-10/100 (Krizhevsky, 2009), STL-10 (Coates et al., 2011), RESISC45 (Cheng et al., 2017), PatchCamelyon (Veeling et al., 2018), and Food101 (Bossard et al., 2014). For end-to-end attacks, we train models following *DataComp* small-scale (see Appendix C for full details). We obtain image embeddings from OpenAI's CLIP ViT-L/14 model (Radford et al., 2021). Gradients for TRAK are obtained from a model trained on the full pool dataset $\mathcal{D}$ using contrastive training as in Gadre et al. (2023). For LIRA attacks, we use 256 shadow sets per configuration (see Appendix C for details).

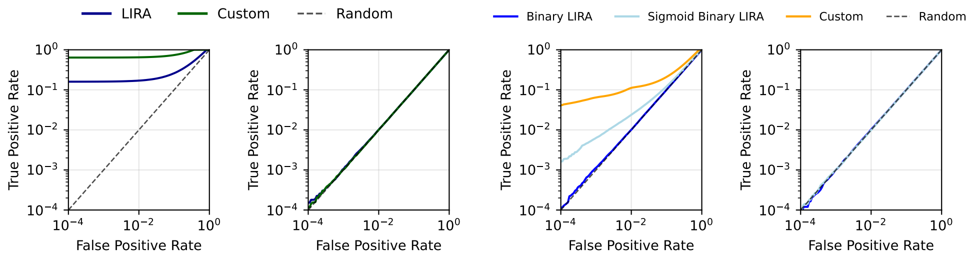

(a) Image-based (b) TRAK (d) Image-based (e) TRAK

(c) Scores (f) Without Scores

Figure 3: **Attack success for curation scores and subsets.** Image-based curation's nearest-neighbor mechanism is highly vulnerable, while TRAK's gradient averaging shows almost no leakage.

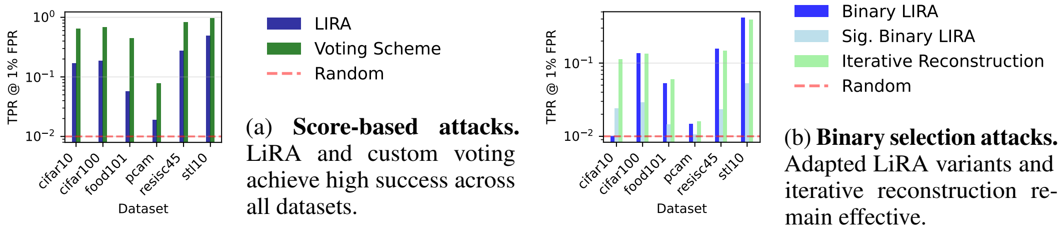

(a) **Score-based attacks.** LiRA and custom voting achieve high success across all datasets.

(b) **Binary selection attacks.** Adapted LiRA variants and iterative reconstruction remain effective.

Figure 4: **Attack success correlates with influence patterns from Figure 2.** Cross-dataset comparison shows TPR at 1% FPR inversely correlates with the percentage of zero-influence targets.

4.1 Attack Performance on Curation Scores

Image-based curation exhibits high attack success rates. The dataset-specific variations in attack success for Image-based curation align with our analysis from Figure 2, namely that datasets with higher influence concentration (fewer targets affecting many public samples) exhibit greater vulnerability. This holds regardless the underlying data type—satellite imagery (RESISC45) with less zero-influence samples is more attackable and medical images (PatchCamelyon) with more zero-influence samples is less attackable than CIFAR10. In contrast, TRAK demonstrates natural protection through its averaging mechanism, giving near-random attack performance (AUC ≈ 0.5) as individual target contributions become diluted through aggregation and dimensionality reduction.

4.2 Attack Performance on Binary Selections

Even when restricted to observing only binary selection patterns, Image-based curation remains vulnerable to membership inference attacks (Section 4). Our iterative reconstruction algorithm successfully recovers the private target set for all samples with non-zero influence, though the large fraction of zero-influence samples provides natural protection for the remaining targets. This success generalizes over various datasets (Figure 4b).

4.3 End-to-End Attacks on Trained Models

The end-to-end attack depends significantly on the target dataset size, so we evaluate TPR at 1% FPR for different target dataset sizes $|\mathcal{T}|$ and various datasets in Figure 5. We show that Image-based curation leads to moderate information leakage across all target dataset sizes, with TPR values up to 21.4% at 1% FPR for RESISC45 at $|\mathcal{T}| = 100$. Targets with non-zero influence are exposed at every target size, creating a bimodal privacy distribution where most samples remain protected while a subset faces significant exposure. TRAK exhibits a different behavior, demonstrating a strong decrease in attack success with growing $|\mathcal{T}|$. This size-dependent vulnerability suggests TRAK may be suitable for large-scale applications but poses significant risks for small, sensitive datasets.

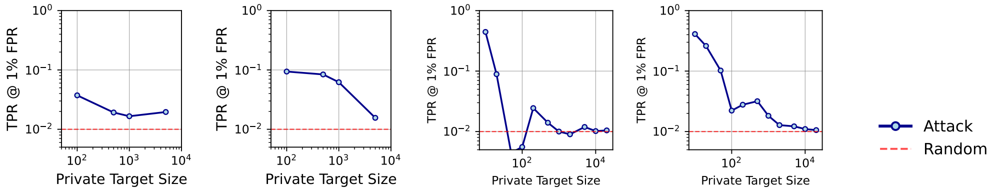

(a) CIFAR-10 (b) RESISC45 (c) CIFAR-10 (d) RESISC45

Image-based TRAK

Figure 5: **End-to-end membership inference success.** Image-based curation shows consistent partial leakage, while TRAK exhibits size-dependent vulnerability.

4.4 Ablations

We perform further ablations on various aspects of our curation setups and analyze their impact on the attack success. We conduct these ablations on attacks against scores, which yield the strongest leakage signal and thus provide the clearest insights into the factors affecting membership inference success. First, we analyze the impact of **the number of dimensions** used for Image-based embeddings and TRAK-based gradient projections. Our results in Figure 37 suggest that for Image-based curation, there is a sweet spot, with the highest leakage at 128 dimensions. TRAK requires enough dimensions ($\geq$ 1,024), below which the attack success drops. Additionally, we show how **target dataset size** impacts attack success. Our results in Figure 32 suggest differences across datasets: *e.g.,* attack success against STL-10 remains near constant while for CIFAR-10, we observe that the success drops as the target dataset size grows. Finally, Figure 36 shows that the **number of shadow models for LiRA** has a varying effect on improving the attack success on different datasets for Image-based curation: *e.g.,* double the number of shadow models from 128 to 256 for CIFAR-10 increases AUC by 10% while for PCAM only for 1%. For TRAK, we do not observe any improvement in attack success when adding more shadow models. We present the full results over all ablations in Appendix E.

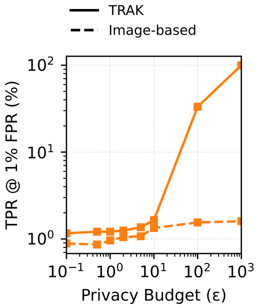

Figure 6: Attack success versus ε for CIFAR-10 ($|\mathcal{T}| = 1000$).

5 Mitigating Privacy Leakage

To mitigate privacy leakage, we adapt curation methods to yield (ε, δ)-Differential Privacy (DP) guarantees via the Gaussian mechanism (Dwork et al., 2006a;b). For **DP Image-based curation** we compute the distance to the DP mean instead of the nearest neighbor of the target dataset. For **DP TRAK-based curation** we privatize the mean gradient computation, similar to Abadi et al. (2016). Appendix D.1 details the algorithms. Figure 6 shows the attack success on the curation scores for our private adaptations. We note that for Image-based curation, replacing the nearest neighbor scores with a mean (without DP) already drops the TPR at 1% FPR from 98.4% to 1.6%. For TRAK-based curation, as we use averaged gradients to perform curation, stricter guarantees are required to reduce the attack success. Appendix D.2 shows that **removing the most vulnerable samples** does not prevent leakage, exhibiting a *privacy onion effect* (Carlini et al., 2022b) for Image-based curation.

6 Discussion and Conclusion

Our work demonstrates that data curation pipelines can leak membership information about the target datasets, exposing privacy risks at every stage, from curation scores and curated subset to the final trained model. Image-based nearest-neighbor methods are particularly vulnerable, and even state-of-the-art approaches like TRAK expose privacy risks for small target sets. Our discovered risks become practically relevant when adversaries can introduce manipulated samples in the curation pool, which is the case when the pool is simply crawled from the internet. This highlights that, as curation becomes central to ML, we need novel curation methods with dedicated safeguards, such as DP, to reduce potential leakage throughout the entire data curation pipeline.

Ethics statement

Our work demonstrates privacy vulnerabilities in data curation methods. We conduct this research to identify and quantify these issues before they can be exploited maliciously, enabling the development of privacy-preserving methods. Our attacks require specific capabilities like injecting target-specific and modified samples into public datasets, which limit their immediate applicability and provide time to implement countermeasures.

Reproducibility statement

Reproducing our results is possible from the information provided, and we support reproduction through the release of all our attack implementations in the supplemental code, as well as providing more detail on the algorithms in the appendix. What hinders reproduction is the computational cost associated with running curation and training algorithms on dataset sizes that are relevant to the topic of data curation. We argue that this is a) to some extent unavoidable and b) our introduction of suitable proxy metrics that eliminate the need to train models improves reproducibility significantly.

References

Martin Abadi, Andy Chu, Ian Goodfellow, H. Brendan McMahan, Ilya Mironov, Kunal Talwar, and Li Zhang. Deep Learning with Differential Privacy. In *Proceedings of the 2016 ACM SIGSAC Conference on Computer and Communications Security*, pp. 308–318, Vienna Austria, 2016. ACM. ISBN 978-1-4503-4139-4. doi: 10.1145/2976749.2978318. URL https://dl.acm.org/doi/10.1145/2976749.2978318.

Meenatchi Sundaram Muthu Selva Annamalai, Borja Balle, Emiliano De Cristofaro, and Jamie Hayes. To Shuffle or not to Shuffle: Auditing DP-SGD with Shuffling, 2024. URL https://arxiv.org/abs/2411.10614.

Kyriakos Axiotis and Maxim Sviridenko. Iterative hard thresholding with adaptive regularization: Sparser solutions without sacrificing runtime. In Kamalika Chaudhuri, Stefanie Jegelka, Le Song, Csaba Szepesvári, Gang Niu, and Sivan Sabato (eds.), *International Conference on Machine Learning, ICML 2022, 17-23 July 2022, Baltimore, Maryland, USA*, volume 162 of *Proceedings of Machine Learning Research*, pp. 1175–1197. PMLR, 2022. URL https://proceedings.mlr.press/v162/axiotis22a.html.

Lukas Bossard, Matthieu Guillaumin, and Luc Van Gool. Food-101 – Mining Discriminative Components with Random Forests. In David Fleet, Tomas Pajdla, Bernt Schiele, and Tinne Tuytelaars (eds.), *Computer Vision – ECCV 2014*, pp. 446–461, Cham, 2014. Springer International Publishing. ISBN 978-3-319-10599-4. doi: 10.1007/978-3-319-10599-4_29.

Nicholas Carlini and Andreas Terzis. Poisoning and backdooring contrastive learning. In *The Tenth International Conference on Learning Representations, ICLR 2022, Virtual Event, April 25-29, 2022*. OpenReview.net, 2022. URL https://openreview.net/forum?id=iC4UHbQ01Mp.

Nicholas Carlini, Steve Chien, Milad Nasr, Shuang Song, Andreas Terzis, and Florian Tramèr. Membership inference attacks from first principles. In *43rd IEEE Symposium on Security and Privacy, SP 2022, San Francisco, CA, USA, May 22-26, 2022*, pp. 1897–1914. IEEE, 2022a. doi: 10.1109/SP46214.2022.9833649. URL https://doi.org/10.1109/SP46214.2022.9833649.

Nicholas Carlini, Matthew Jagielski, Chiyuan Zhang, Nicolas Papernot, Andreas Terzis, and Florian Tramer. The privacy onion effect: Memorization is relative. *Advances in Neural Information Processing Systems*, 35:13263–13276, 2022b.

Nicholas Carlini, Matthew Jagielski, Christopher A. Choquette-Choo, Daniel Paleka, Will Pearce, Hyrum Anderson, Andreas Terzis, Kurt Thomas, and Florian Tramèr. Poisoning Web-Scale Training Datasets is Practical. In *2024 IEEE Symposium on Security and Privacy (SP)*, pp. 407–425, 2024. doi: 10.1109/SP54263.2024.00179. URL https://ieeexplore.ieee.org/abstract/document/10646610. ISSN: 2375-1207.

Gong Cheng, Junwei Han, and Xiaoqiang Lu. Remote sensing image scene classification: Benchmark and state of the art. *Proceedings of the IEEE*, 2017. doi: 10.1109/JPROC.2017.2675998.

Mehdi Cherti and Romain Beaumont. Clip benchmark, 2025. URL https://doi.org/10.5281/zenodo.15403103.

Adam Coates, Andrew Ng, and Honglak Lee. An Analysis of Single-Layer Networks in Unsupervised Feature Learning. In *Proceedings of the Fourteenth International Conference on Artificial Intelligence and Statistics*, pp. 215–223. JMLR Workshop and Conference Proceedings, 2011. URL https://proceedings.mlr.press/v15/coates11a.html. ISSN: 1938-7228.

Together Computer. RedPajama: an open dataset for training large language models, October 2023. URL https://github.com/togethercomputer/RedPajama-Data.

DatalogyAI. DatologyAI: Train Better Models, Faster and Smaller. URL https://www.datologyai.com.

Alexey Dosovitskiy, Lucas Beyer, Alexander Kolesnikov, Dirk Weissenborn, Xiaohua Zhai, Thomas Unterthiner, Mostafa Dehghani, Matthias Minderer, Georg Heigold, Sylvain Gelly, Jakob Uszkoreit, and Neil Houlsby. An Image is Worth 16x16 Words: Transformers for Image Recognition at Scale, June 2021. URL http://arxiv.org/abs/2010.11929. arXiv:2010.11929 [cs].

Cynthia Dwork, Krishnaram Kenthapadi, Frank McSherry, Ilya Mironov, and Moni Naor. Our Data, Ourselves: Privacy Via Distributed Noise Generation. In Serge Vaudenay (ed.), *Advances in Cryptology - EUROCRYPT 2006*, pp. 486–503, Berlin, Heidelberg, 2006a. Springer. ISBN 978-3-540-34547-3. doi: 10.1007/11761679_29.

Cynthia Dwork, Frank McSherry, Kobbi Nissim, and Adam Smith. Calibrating Noise to Sensitivity in Private Data Analysis. In Shai Halevi and Tal Rabin (eds.), *Theory of Cryptography*, Lecture Notes in Computer Science, pp. 265–284, Berlin, Heidelberg, 2006b. Springer. ISBN 978-3-540-32732-5. doi: 10.1007/11681878_14.

Logan Engstrom, Axel Feldmann, and Aleksander Madry. Dsdm: Model-aware dataset selection with datamodels. In *Forty-first International Conference on Machine Learning, ICML 2024, Vienna, Austria, July 21-27, 2024*. OpenReview.net, 2024. URL https://openreview.net/forum?id=GC8HkKeH8s.

Samir Yitzhak Gadre, Gabriel Ilharco, Alex Fang, Jonathan Hayase, Georgios Smyrnis, Thao Nguyen, Ryan Marten, Mitchell Wortsman, Dhruba Ghosh, Jieyu Zhang, Eyal Orgad, Rahim Entezari, Giannis Daras, Sarah M. Pratt, Vivek Ramanujan, Yonatan Bitton, Kalyani Marathe, Stephen Mussmann, Richard Vencu, Mehdi Cherti, Ranjay Krishna, Pang Wei Koh, Olga Saukh, Alexander J. Ratner, Shuran Song, Hannaneh Hajishirzi, Ali Farhadi, Romain Beaumont, Sewoong Oh, Alex Dimakis, Jenia Jitsev, Yair Carmon, Vaishaal Shankar, and Ludwig Schmidt. Datacomp: In search of the next generation of multimodal datasets. In Alice Oh, Tristan Naumann, Amir Globerson, Kate Saenko, Moritz Hardt, and Sergey Levine (eds.), *Advances in Neural Information Processing Systems 36: Annual Conference on Neural Information Processing Systems 2023, NeurIPS 2023, New Orleans, LA, USA, December 10 - 16, 2023*, 2023. URL http://papers.nips.cc/paper_files/paper/2023/hash/56332d41d55ad7ad8024aac625881be7-Abstract-Datasets_and_Benchmarks.html.

Xin Gu, Gautam Kamath, and Zhiwei Steven Wu. Choosing public datasets for private machine learning via gradient subspace distance. In *IEEE Conference on Secure and Trustworthy Machine Learning, SaTML 2025, Copenhagen, Denmark, April 9-11, 2025*, pp. 879–900. IEEE, 2025. doi: 10.1109/SATML64287.2025.00054. URL https://doi.org/10.1109/SaTML64287.2025.00054.

William W. Hager. Updating the Inverse of a Matrix. *SIAM Review*, 31(2):221–239, 1989. ISSN 0036-1445. doi: 10.1137/1031049. URL https://epubs.siam.org/doi/10.1137/1031049. Publisher: Society for Industrial and Applied Mathematics.

Andrew Ilyas and Logan Engstrom. MAGIC: Near-Optimal Data Attribution for Deep Learning, 2025. URL https://arxiv.org/abs/2504.16430.

Andrew Ilyas, Sung Min Park, Logan Engstrom, Guillaume Leclerc, and Aleksander Madry. Datamodels: Predicting Predictions from Training Data, 2022. URL https://arxiv.org/abs/2202.00622.

Matthew Jagielski, Milad Nasr, Katherine Lee, Christopher A. Choquette-Choo, Nicholas Carlini, and Florian Tramèr. Students parrot their teachers: Membership inference on model distillation. In Alice Oh, Tristan Naumann, Amir Globerson, Kate Saenko, Moritz Hardt, and Sergey Levine (eds.), *Advances in Neural Information Processing Systems 36: Annual Conference on Neural Information Processing Systems 2023, NeurIPS 2023, New Orleans, LA, USA, December 10 - 16, 2023*, 2023. URL http://papers.nips.cc/paper_files/paper/2023/hash/8b07d224a643b02e7571e083578a86d2-Abstract-Conference.html.

Alex Krizhevsky. Learning Multiple Layers of Features from Tiny Images. 2009.

Jeffrey Li, Alex Fang, Georgios Smyrnis, Maor Ivgi, Matt Jordan, Samir Yitzhak Gadre, Hritik Bansal, Etash Guha, Sedrick Scott Keh, Kushal Arora, Saurabh Garg, Rui Xin, Niklas Muennighoff, Reinhard Heckel, Jean Mercat, Mayee F. Chen, Suchin Gururangan, Mitchell Wortsman, Alon Albalak, Yonatan Bitton, Marianna Nezhurina, Amro Abbas, Cheng-Yu Hsieh, Dhruba Ghosh, Josh Gardner, Maciej Kilian, Hanlin Zhang, Rulin Shao, Sarah M. Pratt, Sunny Sanyal, Gabriel Ilharco, Giannis Daras, Kalyani Marathe, Aaron Gokaslan, Jieyu Zhang, Khyathi Raghavi Chandu, Thao Nguyen, Igor Vasiljevic, Sham M. Kakade, Shuran Song, Sujay Sanghavi, Fartash Faghri, Sewoong Oh, Luke Zettlemoyer, Kyle Lo, Alaaeldin El-Nouby, Hadi Pouransari, Alexander Toshev, Stephanie Wang, Dirk Groeneveld, Luca Soldaini, Pang Wei Koh, Jenia Jitsev, Thomas Kollar, Alex Dimakis, Yair Carmon, Achal Dave, Ludwig Schmidt, and Vaishaal Shankar. Datacomp-lm: In search of the next generation of training sets for language models. In Amir Globersons, Lester Mackey, Danielle Belgrave, Angela Fan, Ulrich Paquet, Jakub M. Tomczak, and Cheng Zhang (eds.), *Advances in Neural Information Processing Systems 38: Annual Conference on Neural Information Processing Systems 2024, NeurIPS 2024, Vancouver, BC, Canada, December 10 - 15, 2024*, 2024a. URL http://papers.nips.cc/paper_files/paper/2024/hash/19e4ea30dded58259665db375885e412-Abstract-Datasets_and_Benchmarks_Track.html.

Zejian Li, Chenye Meng, Yize Li, Ling Yang, Shengyuan Zhang, Jiarui Ma, Jiayi Li, Guang Yang, Changyuan Yang, Zhiyuan Yang, Jinxiong Chang, and Lingyun Sun. LAION-SG: An enhanced large-scale dataset for training complex image-text models with structural annotations, 2024b. URL https://arxiv.org/abs/2412.08580. arXiv: 2412.08580 [cs.CV].

Ilya Loshchilov and Frank Hutter. Decoupled Weight Decay Regularization, January 2019. URL http://arxiv.org/abs/1711.05101. arXiv:1711.05101 [cs].

Saeed Mahloujifar, Luca Melis, and Kamalika Chaudhuri. Auditing f-Differential Privacy in One Run, 2024. URL https://arxiv.org/abs/2410.22235.

Pratyush Maini, Skyler Seto, Richard He Bai, David Grangier, Yizhe Zhang, and Navdeep Jaitly. Rephrasing the web: A recipe for compute and data-efficient language modeling. In Lun-Wei Ku, Andre Martins, and Vivek Srikumar (eds.), *Proceedings of the 62nd Annual Meeting of the Association for Computational Linguistics (Volume 1: Long Papers), ACL 2024, Bangkok, Thailand, August 11-16, 2024*, pp. 14044–14072. Association for Computational Linguistics, 2024. doi: 10.18653/V1/2024.ACL-LONG.757. URL https://doi.org/10.18653/v1/2024.acl-long.757.

B. K. Natarajan. Sparse Approximate Solutions to Linear Systems. *SIAM Journal on Computing*, 24(2):227–234, 1995. ISSN 0097-5397. doi: 10.1137/S0097539792240406. URL https://epubs.siam.org/doi/abs/10.1137/S0097539792240406. Publisher: Society for Industrial and Applied Mathematics.

Sung Min Park, Kristian Georgiev, Andrew Ilyas, Guillaume Leclerc, and Aleksander Madry. TRAK: attributing model behavior at scale. In Andreas Krause, Emma Brunskill, Kyunghyun Cho, Barbara Engelhardt, Sivan Sabato, and Jonathan Scarlett (eds.), *International Conference on Machine Learning, ICML 2023, 23-29 July 2023, Honolulu, Hawaii, USA*, volume 202 of *Proceedings of Machine Learning Research*, pp. 27074–27113. PMLR, 2023. URL https://proceedings.mlr.press/v202/park23c.html.

Guilherme Penedo, Quentin Malartic, Daniel Hesslow, Ruxandra Cojocaru, Alessandro Cappelli, Hamza Alobeidli, Baptiste Pannier, Ebtesam Almazrouei, and Julien Launay. The RefinedWeb dataset for falcon LLM: Outperforming curated corpora with web data, and web data only, 2023. URL https://arxiv.org/abs/2306.01116. arXiv: 2306.01116 [cs.CL].

Guilherme Penedo, Hynek Kydlíček, Loubna Ben allal, Anton Lozhkov, Margaret Mitchell, Colin Raffel, Leandro Von Werra, and Thomas Wolf. The FineWeb datasets: Decanting the web for the finest text data at scale, 2024. URL https://arxiv.org/abs/2406.17557. arXiv: 2406.17557 [cs.CL].

Alec Radford, Jong Wook Kim, Chris Hallacy, Aditya Ramesh, Gabriel Goh, Sandhini Agarwal, Girish Sastry, Amanda Askell, Pamela Mishkin, Jack Clark, Gretchen Krueger, and Ilya Sutskever. Learning transferable visual models from natural language supervision. In Marina Meila and Tong Zhang (eds.), *Proceedings of the 38th International Conference on Machine Learning, ICML 2021, 18-24 July 2021, Virtual Event*, volume 139 of *Proceedings of Machine Learning Research*, pp. 8748–8763. PMLR, 2021. URL http://proceedings.mlr.press/v139/radford21a.html.

ScaleAI. Scale AI. URL https://scale.com.

Reza Shokri, Marco Stronati, Congzheng Song, and Vitaly Shmatikov. Membership inference attacks against machine learning models. In *2017 IEEE Symposium on Security and Privacy, SP 2017, San Jose, CA, USA, May 22-26, 2017*, pp. 3–18. IEEE Computer Society, 2017. doi: 10.1109/SP.2017.41. URL https://doi.org/10.1109/SP.2017.41.

Snorkel. Snorkel AI | Helping model providers and AI development teams push the boundaries of AI. URL https://snorkel.ai/.

Tristan Thrush, Christopher Potts, and Tatsunori Hashimoto. Improving pretraining data using perplexity correlations. In *The Thirteenth International Conference on Learning Representations, ICLR 2025, Singapore, April 24-28, 2025*. OpenReview.net, 2025. URL https://openreview.net/forum?id=huuKoVQnB0.

Bastiaan S. Veeling, Jasper Linmans, Jim Winkens, Taco Cohen, and Max Welling. Rotation equivariant cnns for digital pathology. In Alejandro F. Frangi, Julia A. Schnabel, Christos Davatzikos, Carlos Alberola-López, and Gabor Fichtinger (eds.), *Medical Image Computing and Computer Assisted Intervention - MICCAI 2018 - 21st International Conference, Granada, Spain, September 16-20, 2018, Proceedings, Part II*, volume 11071 of *Lecture Notes in Computer Science*, pp. 210–218. Springer, 2018. doi: 10.1007/978-3-030-00934-2_24. URL https://doi.org/10.1007/978-3-030-00934-2_24.

Shanshan Wu, Zheng Xu, Yanxiang Zhang, Yuanbo Zhang, and Daniel Ramage. Prompt Public Large Language Models to Synthesize Data for Private On-device Applications, 2024. URL https://arxiv.org/abs/2404.04360.

Da Yu, Sivakanth Gopi, Janardhan Kulkarni, Zinan Lin, Saurabh Naik, Tomasz Lukasz Religa, Jian Yin, and Huishuai Zhang. Selective pre-training for private fine-tuning. *Trans. Mach. Learn. Res.*, 2024, 2024. URL https://openreview.net/forum?id=y3u8OpPHxz.

A Curation Methods

Table 2: Overview of Curation Methods

Method	Description	Score Function
Image-based	Identifies relevant pool data using image embeddings	$s(x) = \max_{t\in\mathcal{T}} \cos(\phi(x), \phi(t))$ where $\phi(\cdot)$ is the embedding function
TRAK	Computes attribution scores via projected gradients to identify influential pool samples	$s(x) = \frac{1}{\lvert\mathcal{T}\rvert}\sum_{t\in\mathcal{T}} \Phi(x)^T G_t$ where Φ are projected and out-to-loss-scaled features

A.1 Image-Based Scoring

We employ Image-based nearest neighbor distances inspired by Gadre et al. (2023). Following the DataComp methodology, we use embeddings from OpenAI's pretrained CLIP ViT-L/14 model (Radford et al., 2021) to compute the image representations $\phi(\cdot)$. For each pool sample $x_i \in \mathcal{D}$, the curation score is computed as the maximum cosine similarity to any target sample in $\mathcal{T}$, *i.e.,* the pool sample is scored based on its closest (most similar) target sample. This nearest-neighbor mechanism creates a deterministic relationship where each pool sample's score is determined by exactly one target sample.

A.2 TRAK

The TRAK algorithm (Park et al., 2023) for computing influence scores is formally presented in Algorithm 2.

Algorithm 2 TRAK Algorithm for Influence Computation

```
Require: Training dataset $\mathcal{D}$, target dataset $\mathcal{T}$, model $f_\theta$, projection dimension $d_{\text{proj}}$
Ensure: Influence scores $s$ of training samples on target samples
    $\mathbf{G}_{\text{train}} \leftarrow \nabla_\theta f_\theta(\mathcal{D})$                                ▷ Gradients for training data
    $\boldsymbol{\alpha}_{\text{train}} \leftarrow \nabla_{f_\theta} \mathcal{L}(\mathcal{D}, f_\theta)$                          ▷ Output-to-loss gradients
    $\mathbf{G}_{\text{target}} \leftarrow \nabla_\theta f_\theta(\mathcal{T})$                               ▷ Gradients for target data
    $\mathbf{P} \leftarrow \text{RandomProjectionMatrix}(\dim(\theta), d_{\text{proj}})$      ▷ Typically Rademacher
    $\mathbf{G}_{\text{train}} \leftarrow \mathbf{G}_{\text{train}}\mathbf{P}$                                  ▷ Project training gradients
    $\mathbf{G}_{\text{target}} \leftarrow \mathbf{G}_{\text{target}}\mathbf{P}$                                ▷ Project target gradients
    $\mathbf{X}^T\mathbf{X} \leftarrow \mathbf{G}_{\text{train}}^T\mathbf{G}_{\text{train}}$                              ▷ Compute Gram matrix
    $\boldsymbol{\Phi} \leftarrow \mathbf{G}_{\text{train}} \cdot (\mathbf{X}^T\mathbf{X})^{-1}$                         ▷ Compute features
    $\mathbf{s}_{\text{raw}} \leftarrow \frac{1}{|\mathcal{T}|}\sum_{i=1}^{|\mathcal{T}|} \boldsymbol{\Phi} \cdot \mathbf{G}_{\text{target},i}^T$                 ▷ Raw scores
    $\mathbf{s} \leftarrow \mathbf{s}_{\text{raw}} \odot \boldsymbol{\alpha}_{\text{train}}$                          ▷ Scale by output-to-loss gradients
    return $\mathbf{s}$                                                ▷ Final influence scores
```

B Attacking Curation Scores

B.1 Attack Design Rationale

We design our attacks to exploit the specific mathematical structure of each curation method. While no attack can be proven universally optimal without strong distributional assumptions, our approaches are theoretically grounded and, in the case of Image-based scoring, exploit fundamental limits of what can be inferred from the exposed information.

Method-Agnostic Attacks via LiRA. For general-purpose membership inference, we employ the Likelihood Ratio Attack (LiRA) (Carlini et al., 2022a). This attack is theoretically motivated by the

Neyman-Pearson lemma, which establishes that the likelihood ratio test is optimal for binary hypothesis testing (membership vs. non-membership) under the assumption that the score distributions are known or can be accurately estimated. LiRA provides a principled baseline that makes minimal assumptions about the curation method's internal structure.

We make two key adaptations for curation pipelines. First, we replace shadow *models* with shadow *curation runs*,*i.e.,* instantiations of the curation algorithm using different random subsets of $\mathcal{T}$, s.t. each target sample is part of exactly half of the random subsets. Second, following Jagielski et al. (2023), we filter the curation scores to select only the public sample per target with the maximum difference in expected scores between member and non-member hypotheses (Equation (1)).

This preserves the essential statistical properties needed for LiRA: we can empirically model $P(s|t \in \mathcal{T})$ and $P(s|t \notin \mathcal{T})$ from shadow observations. Figure 7a illustrates the resulting in and out score distributions. We can then formulate a likelihood ratio attack on the curation scores by computing the log-ratio of the in and out score distributions (Equation (3)). Figure 7b illustrates the mapping from measured scores to the resulting membership inference score. Given sufficient shadow sets and correct distributional assumptions (*e.g.,* Gaussian for continuous scores, Bernoulli for binary selections), LiRA approximates the theoretically optimal likelihood ratio test.

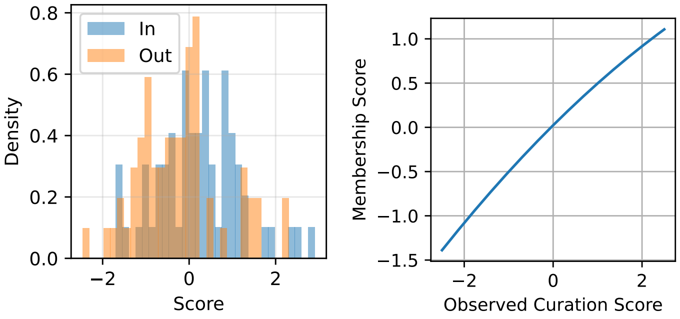

(a) In and out score distributions. (b) Membership inference score.

Figure 7: **LiRA can be adapted to curation pipelines.** (a) We can empirically model $P(s|t \in \mathcal{T})$ and $P(s|t \notin \mathcal{T})$ from shadow observations. (b) We can then compute membership inference scores based on a likelihood ratio attack by computing the log-ratio of the in and out score distributions.

Image-Based Curation: Exploiting Deterministic Structure. For Image-based scoring with nearest-neighbor retrieval ($s(x) = \max_{t \in \mathcal{T}} \cos(\phi(x), \phi(t))$), the max operation creates a *deterministic* function where each pool sample's score is determined by exactly one target sample: its nearest neighbor. This structure enables perfect reverse-engineering: given $s(x)$ and the embeddings, we can identify which $t^* \in \mathcal{T}$ was responsible via $t^* = \arg\min_t |\cos(\phi(x), \phi(t)) - s(x)|$.

Our custom voting attack exploits this theoretical limit, since only nearest-neighbor relationships are exposed, and our attack recovers exactly these relationships. Positive votes accumulate for targets that are nearest neighbors to pool samples, while negative votes identify targets that would have produced higher scores if present. This is fundamentally more powerful than LiRA because it does not rely on distributional assumptions or shadow set approximations; it deterministically extracts the membership signal embedded in the nearest-neighbor structure.

The attack's effectiveness is constrained only by: (1) the sparsity of nearest-neighbor relationships (many targets may not be nearest neighbors to any pool sample, as shown in the main paper), and (2) numerical precision in matching scores to similarities. Unlike LiRA, which requires many shadow sets to approximate distributions, our deterministic attack needs only the scoring function's mathematical structure and embedding access.

B.1.1 ORACLE ATTACK SETUP

To establish an upper bound on attack performance for Image-based scoring, we define an oracle attack that leverages perfect knowledge of the curation mechanism. The oracle operates under the following membership scoring scheme for each target sample $t \in \mathcal{T}$:

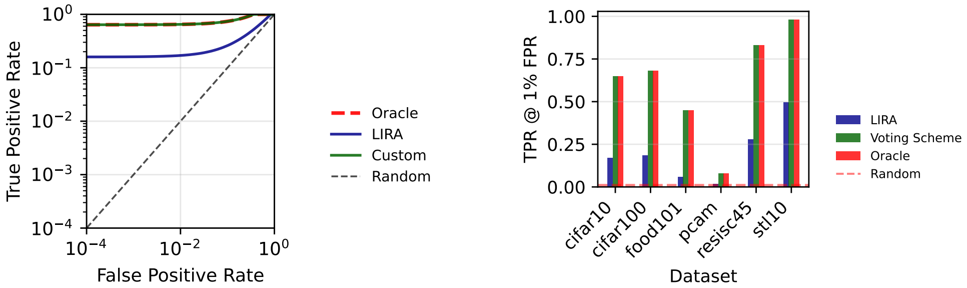

(a) CIFAR-10

(b) Multiple Datasets

Figure 8: **Our custom attack on Image-based scores matches oracle performance.** With access to the scores, the attack achieves the same utility as the oracle attack.

$$\text{membership\_score}(t) = \begin{cases} 1 & \text{if } t \text{ is the nearest neighbor of any pool sample} \\ 0 & \text{if } \exists x \in \mathcal{D} : \cos(\phi(x), \phi(t)) > s(x) \\ 0.5 & \text{otherwise (no influence on scores)} \end{cases} \tag{17}$$

The rationale for this scoring scheme is as follows:

- **Score 1 (Member):** If a target sample t is responsible for the observed score of at least one pool sample (*i.e.,* it is the nearest neighbor in $\mathcal{T}$ for that pool sample), then the oracle has definitive evidence that $t \in \mathcal{T}_{\text{sel}}$.
- **Score 0 (Non-member):** If the oracle can identify pool samples where the similarity to t exceeds the observed score, this indicates that t would have produced a higher score if it were in $\mathcal{T}_{\text{sel}}$. Since it did not, the oracle can definitively conclude that $t \notin \mathcal{T}_{\text{sel}}$.
- **Score 0.5 (Unknown):** For target samples that have no observable influence on any pool scores—neither as nearest neighbors nor as potential higher-scoring alternatives—even the most powerful oracle can only guess their membership status uniformly at random.

This oracle attack represents the theoretical maximum achievable performance given the information exposed by the Image-based scoring mechanism. As shown in Figure 8, our deterministic voting attack matches oracle performance when scores are available, confirming that it successfully extracts all membership information embedded in the nearest-neighbor structure.

TRAK: Compressed Sensing for Averaged Signals. TRAK scores are computed as $s(x) = \frac{1}{|\mathcal{T}|}\sum_{t\in\mathcal{T}} \Phi(x)^\top G_t$, averaging gradient contributions projected to a low-dimensional space from all targets. This averaging *diffuses* individual membership signals, preventing the deterministic reverse-engineering that succeeds for Image-based methods.

Recovering which targets contributed to averaged scores is a *sparse recovery* problem: given the observation $s \in \mathbb{R}^{|\mathcal{D}|}$ and the measurement matrix $\Phi^\top G \in \mathbb{R}^{|\mathcal{D}|\times|\mathcal{T}|}$, we seek the sparse indicator vector $\mathcal{T}_{\text{sel}} \in \{0,1\}^{|\mathcal{T}|}$ such that $s \approx \Phi^\top G \mathcal{T}_{\text{sel}}$. This is a compressed sensing problem that has been extensively studied in signal processing and optimization literature.

We employ Orthogonal Matching Pursuit (OMP) and Iterative Hard Thresholding (IHT) (Axiotis & Sviridenko, 2022)—greedy algorithms known to provide near-optimal solutions under certain conditions. These represent the state-of-the-art for practical sparse recovery. Theoretically optimal attacks would require solving the ℓ_0-minimization problem exactly, which is NP-hard (Natarajan, 1995). Brute-force search over all $\binom{|\mathcal{T}|}{|\mathcal{T}_{\text{sel}}|}$ possible target subsets is computationally infeasible for realistic dataset sizes (*e.g.,* $\binom{50000}{5000} \approx 10^{7000}$ possibilities).

In practice, we find that even these theoretically-grounded compressed sensing attacks fail to meaningfully outperform LiRA on TRAK. This empirical result suggests that the averaging operation in TRAK provides inherent protection by spreading signal across many dimensions, making sparse recovery ill-conditioned. The attack success becomes dependent on $|\mathcal{T}|$: smaller target sets (common in sensitive domains) concentrate signal and become more vulnerable, while larger sets benefit from stronger averaging.

B.2 Method-Agnostic Attacks

To attack the curation methods, we employ the likelihood-ratio attack (LiRA) from Carlini et al. (2022a). We initialize $N = 256$ shadow models. Each of those uniformly curates for a random subset of the target dataset, s.t., each target sample is used in exactly half of the shadow models. Furthermore, we perform 25 independent curation runs on random subsets that we will attack.

To analyze the attacakbility of a target sample, we group the shadow model scores into those that contained the target sample $\mathbf{S}_{\text{in}}$ and those that did not $\mathbf{S}_{\text{out}}$. We then average over the shadow models, giving us two vectors of pool scores $\mathbf{s}_{\text{in}}$ and $\mathbf{s}_{\text{out}}$. As many of those scores will probably not give us meaningful membership signals (Jagielski et al., 2023), we first find the index of the pool score that has the largest average difference, *i.e.,* $i = \arg\max |\mathbf{s}_{\text{in}} - \mathbf{s}_{\text{out}}|$. We then fit a Gaussian to the distribution of $\mathbf{S}_{i,\text{in}}$ and $\mathbf{S}_{i,\text{out}}$, giving us two distributions $P_{\text{in}}(s)$ and $P_{\text{out}}(s)$. We can then compute the log-ratio of the of the ith pool score to the two distributions, giving us the LiRA score.

To perform the attack without access to the scores, we replace the scores with binary signals, indicating whether a particular pool sample would be in the selected partition of the shadow models. The **binarized LiRA** computes the mean of those binary signals and computes the difference in bernoulli log-probability mass functions.

B.3 Image-Based Scoring

We recall that for Image-based scoring, the score for each sample in $\mathcal{D}$ is only influenced by the nearest neighbour in $\mathcal{T}$. Therefore, we analyse how many pool samples each target sample is the nearest neighbour for.

Given a pool sample $x \in \mathcal{D}$ with target score $s(x)$, we can determine which target sample $t \in \mathcal{T}$ was responsible for this score through the following attack:

1. Normalize the embeddings: $\hat{x} = \frac{\phi(x)}{\|\phi(x)\|_2}$ and $\hat{t} = \frac{\phi(t)}{\|\phi(t)\|_2}$ for all $t \in \mathcal{T}$
2. Compute similarities: $\text{sim}(x, t) = \hat{x}^T \hat{t}$ for all $t \in \mathcal{T}$
3. Find target with matching score: $t^* = \arg\min_{t \in \mathcal{T}} |\text{sim}(x, t) - s(x)|$
4. For each target t, assign votes:

$$v(t) = \begin{cases} 1 & \text{if } t = t^* \\ -1 & \text{if } \text{sim}(x, t) > s(x) \\ 0 & \text{otherwise} \end{cases}$$

The voting scheme reveals membership in $\mathcal{T}$ through positive votes: if a target sample receives positive votes, it was used to compute the score of at least one pool sample. Negative votes indicate that this target sample could have given a higher score than what was observed, implying it was not used in the curation.

Selection-Based Attack. When we only have access to the selected pool samples $\tilde{\mathcal{D}} \subseteq \mathcal{D}$ but not their scores, we can still reconstruct the target dataset through an iterative elimination process:

1. Initialize $\mathcal{T}_0 = \mathcal{T}$ as the full target dataset, $\mathcal{R} = \emptyset$ as the set of removed samples, and voting scores $\mathbf{v} = \mathbf{0}$
2. At each iteration i:
   (a) Identify target-missing and target-exclusive samples:
      - Target-missing: $\mathcal{M}_i = \tilde{\mathcal{D}}_i \setminus \tilde{\mathcal{D}}_{\text{target}}$ (selected by us but not target)
      - Target-exclusive: $\mathcal{E}_i = \tilde{\mathcal{D}}_{\text{target}} \setminus \tilde{\mathcal{D}}_i$ (selected by target but not us)

   (b) Find nearest neighbors in remaining targets:
      - For target-missing: $\mathcal{N}_i^- = \text{NN}(\mathcal{M}_i, \mathcal{T}_i)$

Algorithm 3 Image-based Scores MIA

```
Input: Dataset embeddings $\{\phi(x)\}_{x\in\mathcal{D}}$, target embeddings $\{\phi(t)\}_{t\in\mathcal{T}}$, target scores $\mathbf{s}$
Output: Votes $v(t)$ for each target $t \in \mathcal{T}$
Initialize $\forall_{t\in\mathcal{T}} : v(t) = 0$
Normalize all target embeddings: $\hat{\mathbf{t}} = \frac{\phi(t)}{\|\phi(t)\|_2}$ for all $t \in \mathcal{T}$
for each sample $x \in \mathcal{D}$ do
    Normalize the query embedding: $\hat{\mathbf{x}} = \frac{\phi(x)}{\|\phi(x)\|_2}$
    Compute similarities: $\text{sim}(x, t) = \hat{\mathbf{x}}^T\hat{\mathbf{t}}$ for all $t \in \mathcal{T}$
    Find target with matching score: $t^* = \arg\min_{t\in\mathcal{T}} |\text{sim}(x, t) - s(x)|$
    for each target $t \in \mathcal{T}$ do
        if $t = t^*$ then
            $v(t) = v(t) + 1$
        else if $\text{sim}(x, t) > s(x)$ then
            $v(t) = v(t) - 1$
        end if
    end for
end for
```

   - For target-exclusive: $\mathcal{N}_i^+ = \text{NN}(\mathcal{E}_i, \mathcal{T}_i)$

(c) Update votes:
   - $\mathbf{v}[\mathcal{N}_i^-] \leftarrow \mathbf{v}[\mathcal{N}_i^-] - 1$ (negative for likely non-members)
   - $\mathbf{v}[\mathcal{N}_i^+] \leftarrow \mathbf{v}[\mathcal{N}_i^+] + 1$ (positive for likely members)

(d) Update removed set: $\mathcal{R} = \{t \in \mathcal{T} : \mathbf{v}[t] < 0\}$

(e) Update remaining targets: $\mathcal{T}_{i+1} = \mathcal{T} \setminus \mathcal{R}$

(f) Recompute pool selection: $\tilde{\mathcal{D}}_{i+1} = \text{TopK}(\text{NN-Sim}(\mathcal{D}, \mathcal{T}_{i+1}), k)$

(g) Compute Jaccard similarity: $J_i = \frac{|\tilde{\mathcal{D}}_{i+1} \cap \tilde{\mathcal{D}}_{\text{target}}|}{|\tilde{\mathcal{D}}_{i+1} \cup \tilde{\mathcal{D}}_{\text{target}}|}$

3. Stop when either:
   - Perfect reconstruction: $J_i = 1$
   - No improvement: $J_i - J_{i-p} < \epsilon$ for patience p and threshold ϵ

The attack maintains a voting score for each target sample. Negative votes suggest the target sample is causing overselection of pool samples that are no in $\mathcal{T}_{\text{Sel.}}$, while positive votes indicate the target sample helps select pool samples that are also in $\mathcal{T}_{\text{Sel.}}$. The ROC-AUC of these votes against true membership provides a measure of attack success.

B.4 TRAK

TRAK computes the scores for all pool samples $\mathbf{s} \in \mathcal{R}^{|\mathcal{D}|}$ as

$$\mathbf{s} = \frac{1}{|\mathcal{T}|} \sum_{t\in\mathcal{T}} \mathbf{\Phi}^T \mathbf{G}_t \tag{18}$$

Following the DsDm methodology (Engstrom et al., 2024), we first train a CLIP model on the full pool dataset $\mathcal{D}$ to obtain a reference model. We then obtain the gradients $\mathbf{G}_t$ and $\mathbf{\Phi}$ from this model by computing the per-sample zero-shot gradients—the gradients obtained by minimizing the classification loss of the linear zero-shot classifier obtained by embedding caption-templates (Cherti & Beaumont, 2025). The curation score for each pool sample is the average of its TRAK attribution scores across all target samples $t \in \mathcal{T}$, capturing how influential that pool sample would be for improving performance on the target dataset.

Since the target model does not use the entire target dataset, but instead an unknown subset $\mathcal{T}_{\text{sel}} \subseteq \mathcal{T}$, the target scores are computed as

$$\mathbf{s}_{\mathcal{T}_{\text{sel}}} = \frac{1}{|\mathcal{T}_{\text{sel}}|} \sum_{t\in\mathcal{T}_{\text{sel}}} \mathbf{\Phi}^T \mathbf{G}_t \tag{19}$$

where $\mathbf{G}_{\mathcal{T}_{\text{sel}}} \in \mathbb{R}^{d\times|\mathcal{T}_{\text{sel}}|}$ is the matrix of the target gradients for the selected target samples.

Recovering $\mathcal{T}_{\text{sel}}$ from $\mathbf{s}_{\mathcal{T}}$ constitutes a subset-sum problem, which is NP-hard (Natarajan, 1995). We know about $\mathcal{T}_{\text{sel}}$ that it is a subset of $\mathcal{T}$.

B.4.1 ORTHOGONAL MATCHING PURSUIT

Hence, we can formulate this as a standard compressed sensing problem with the formulation

$$\mathbf{s}_{\mathcal{T}_{\text{sel}}} = \mathbf{\Phi}^T \mathbf{G} \mathbf{T}_{\text{sel}} \tag{20}$$

where $\mathbf{T}_{\text{sel}} \in \mathbb{R}_+^{|\mathcal{T}|}$ is a $|\mathcal{T}_{\text{sel}}|-$sparse vector that performs the equivalance of a masked mean computation. We then recover the standard compressed sensing problem

$$\min_{\mathbf{T}_{\text{sel}} \in \mathbb{R}_+^{|\mathcal{T}|}} \|\mathbf{T}_{\text{sel}}\|_0 \quad \text{s.t.} \quad \mathbf{\Phi}^T \mathbf{G} \mathbf{T}_{\text{sel}} = \mathbf{s}_{\mathcal{T}_{\text{sel}}} \tag{21}$$

where $\|\mathbf{T}_{\text{sel}}\|_0$ is the ℓ_0-"norm" of $\mathbf{T}_{\text{sel}}$, *i.e.*, the number of non-zero elements in $\mathbf{T}_{\text{sel}}$. We approach this problem using the greedy orthogonal matching pursuit (OMP) algorithm and adaptively regularized iterative hard thresholding (IHT) (Axiotis & Sviridenko, 2022).

B.4.2 LEAST SQUARES FORMULATION

We solve for the membership indicator via least squares. Let $\mathbf{X} \in \mathbb{R}^{N\times d}$ denote the pool features ($\mathbf{\Phi}$) and $\mathbf{Y} \in \mathbb{R}^{n\times d}$ the target gradients ($\mathbf{G}^T$). The TRAK scores satisfy

$$\mathbf{s} = \frac{1}{k} \sum_{i\in\mathcal{T}_{\text{sel}}} \mathbf{X}\mathbf{Y}_i^T = \mathbf{X}\mathbf{Y}^T\mathbf{m} \tag{22}$$

where $\mathbf{m} \in \{0, 1/k\}^n$ is the mean operator encoding membership, with $k = |\mathcal{T}_{\text{sel}}|$ non-zero entries indicating which targets are in $\mathcal{T}_{\text{sel}}$. To avoid materializing $\mathbf{X}\mathbf{Y}^T \in \mathbb{R}^{N\times n}$, we multiply both sides from the left by $\mathbf{X}^T$:

$$\mathbf{X}^T\mathbf{s} = \mathbf{X}^T\mathbf{X}\mathbf{Y}^T\mathbf{m}. \tag{23}$$

Since $\mathbf{X}^T\mathbf{X} \in \mathbb{R}^{d\times d}$ and $(\mathbf{X}^T\mathbf{X})\mathbf{Y}^T \in \mathbb{R}^{d\times n}$ are tractable, we avoid materializing the (N, n) matrix. We solve the least squares problem

$$\underset{\mathbf{m}\in\mathbb{R}^n}{\text{minimize}} \quad \|\mathbf{X}^T\mathbf{X}\mathbf{Y}^T\mathbf{m} - \mathbf{X}^T\mathbf{s}\|_2^2 \tag{24}$$

for $\mathbf{m}$. The membership scores are then given by $\mathbf{s}_{\text{lstsq}} = \mathbf{m}^*$, where $\mathbf{m}^*$ is the optimal solution.

B.5 COMBINING VOTING AND LIRA ATTACKS

We analyze whether the voting-based attack for Image-based scoring and the LiRA attack provide complementary signals that can be combined for improved membership inference. The attacks exploit different aspects of the curation mechanism: voting exploits the deterministic nearest-neighbor structure, while LiRA models score distributions from shadow curation runs. Correlation analysis reveals that LiRA and voting scores have low Pearson correlation ($\rho \approx 0.3$).

We combine the two attack scores via weighted averaging:

$$s_{\text{combined}}(t) = w \cdot s_{\text{LiRA}}(t) + (1 - w) \cdot s_{\text{voting}}(t) \tag{25}$$

where $s_{\text{LiRA}}(t)$ and $s_{\text{voting}}(t)$ are normalized to $[0, 1]$, and $w \in [0, 1]$ controls the weighting. We evaluate $w \in \{0, 0.25, 0.5, 0.75, 1.0\}$ to identify the optimal combination.

Figure 9 shows ROC curves for the individual and combined attacks. The combined method does not improve over voting alone. Since LiRA substantially underperforms voting on Image-based scoring (AUC ≈ 0.6 vs. ≈ 0.95) and the voting-based attack already matches the oracle attack performance (Figure 8), LiRA contributes mostly noise when combined.

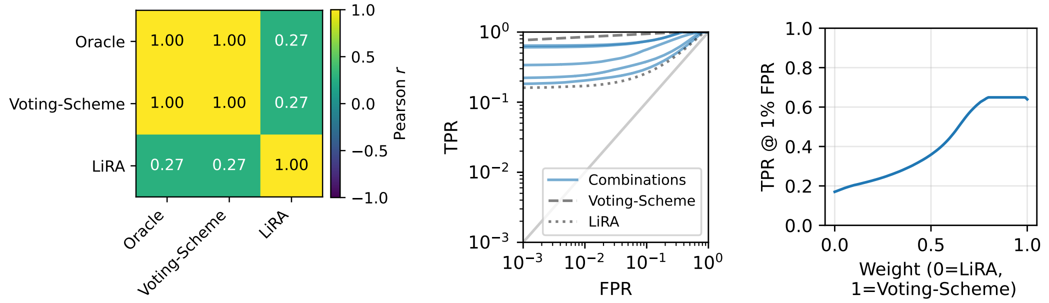

(a) Score correlation analysis

(b) Combined ROC

(c) Combined TPR at 1% FPR

Figure 9: **Combining voting and LiRA does not improve attack performance.** (a) Scatter plot showing correlation between LiRA and voting scores reveals low correlation ($\rho = 0.27$). (b) ROC curves for the combined attack and (c) TPR at 1% FPR for different weightings of the two attacks. We show that the combined attack does not improve over voting alone.

C Attacking Models Trained on Curated Data

C.1 Model Training Details

All end-to-end attack experiments train CLIP models following the DataComp small-scale benchmark (Gadre et al., 2023). We provide the complete training configuration below: We use the Vision Transformer ViT-B-32 architecture (Dosovitskiy et al., 2021) for all experiments. Models are trained with the AdamW optimizer (Loshchilov & Hutter, 2019) with the following hyperparameters:

- Learning rate: 5×10^{-4} with cosine decay schedule
- Linear warmup: 500 steps
- Weight decay: 0.2
- Beta coefficients: $\beta_1 = 0.9$, $\beta_2 = 0.98$
- Gradient clipping: maximum norm of 1.0
- Batch size: 1024
- Precision: Automatic mixed precision (AMP)

Training Budget. All models are trained for a fixed budget of 10M samples. The number of epochs is adjusted based on the curated pool size, *e.g.,* a pool of 100k samples results in 100 epochs, while a pool of 1M samples results in 10 epochs. This ensures all models receive equivalent amounts of training regardless of curation pool size.

Training Data. Models are trained exclusively on the curated subset $\tilde{\mathcal{D}}$ selected from CommonPool (small). They are *never* trained on the private target data $\mathcal{T}$ directly—they only benefit from curation performed using $\mathcal{T}$.

C.2 Image-Based

Image-based curation scores each pool sample $x \in \mathcal{D}$ based on its maximum similarity to any target sample:

$$s(x) = \max_{t \in \mathcal{T}} \cos(\phi(x), \phi(t)) \tag{26}$$

where $\phi(\cdot)$ is the CLIP embedding function. This creates a one-to-many correspondence mapping between targets and pool samples.

The key insight: When a target t^* is included in the victim's subset $\mathcal{T}_{\text{victim}}$, all pool samples for which t^* is the nearest neighbor will receive higher scores and may cross the selection threshold.

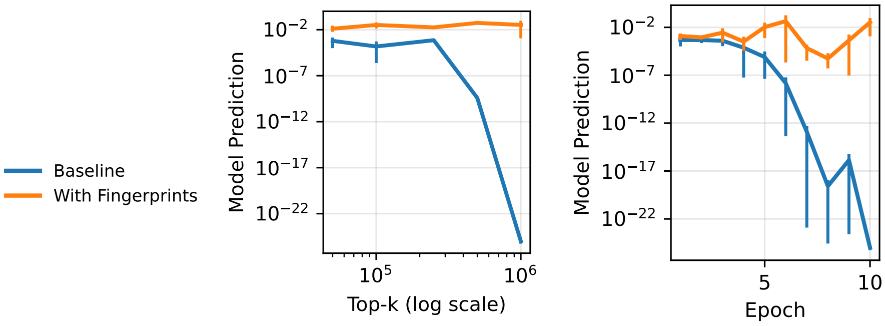

(a) Effect of training set size (b) Signal evolution during training

Figure 10: **Mislabeled images leave a measurable fingerprint in the trained model.** We fix the number of fingerprints at 5 and measure probability on the mislabeled concept. (a) The signal remains detectable even as the training set grows to 1,000,000 samples (0.0005% fingerprint rate), though variance increases. Non-fingerprinted models consistently produce near-zero signal, enabling reliable fingerprint detection. (b) The fingerprint signal strengthens with additional training epochs.

We note that by default most target samples do not affect any target samples, as Figure 2 shows. But, we assume the adversary can inject samples with embeddings $X = \{x_1, \ldots, x_M\} \subset \mathbb{R}^d$ into the pool to probe membership.

Algorithm 4 Image-based Correspondence Mapping

```
1: Input: Candidate embeddings $\Phi_C$, target pool embeddings $\Phi_\mathcal{T}$, mixing parameter $\alpha$
2: Phase 1: Find correspondences
3: For each target $t \in \mathcal{T}$:
4:     Find $k$ candidate nearest neighbors: $\text{NN}_k(t) = \{x_1, \ldots, x_k\}$
5:     Compute attraction score: $a_i = \cos(\phi(t), \phi(x_i))$ (similarity to target)
6:     Compute repulsion score: $r_i = \max_{t' \neq t} \cos(\phi(t'), \phi(x_i))$ (similarity to other targets)
7:     Combined score: $s_i = (1 - \alpha) \cdot a_i + \alpha \cdot r_i$
8:     Select best match: $x^* = \arg\max_{x \in \text{NN}_k(t)} s_i$
9:     Store mapping: $\mathcal{M}(t) = x^*$
10: Phase 2: Identify correspondence uniqueness
11: For each selected candidate $x \in \{x^* : x^* = \mathcal{M}(t) \text{ for some } t\}$:
12:     Count targets mapping to it: $|\mathcal{M}^{-1}(x)| = |\{t : \mathcal{M}(t) = x\}|$
13: Output: Correspondence mapping $\mathcal{M}$ and uniqueness counts $|\mathcal{M}^{-1}(x)|$
```

For each candidate sample x, we compute its baseline percentile against the full target pool:

$$p_0(x) = \text{percentile}\left(\max_{t \in \mathcal{T}} \cos(\phi(x), \phi(t))\right) \tag{27}$$

This represents the expected ranking when the target randomly selects their subset $\mathcal{T}_{\text{Sel.}}$.

The adversary then marks samples for monitoring based on information potential: For sample x with targets $\mathcal{M}^{-1}(x)$:

$$\text{InfoScore}(x) = \text{CrossingScore}(x) \times \text{UniquenessScore}(x) \tag{28}$$

where:

$$\text{CrossingScore}(x) = \begin{cases} \frac{1}{1+e^{(\tau - p_0(x) - 10)/5}} & \text{if } p_0(x) < \tau \\ 0.1 & \text{if } p_0(x) \geq \tau \end{cases} \tag{29}$$

$$\text{UniquenessScore}(x) = \frac{1}{|\mathcal{M}^{-1}(x)|} \tag{30}$$

Algorithm 5 Image-based End-to-End MIA

```
Input: Fingerprinted samples $\mathcal{F}$, selection observations $\{\text{selected}_x : x \in \mathcal{F}\}$, baseline percentiles $\{p_0^x\}$, selection rate $\rho$
Compute selection threshold: $\tau = (1 - \rho) \times 100$ (e.g., $\pi_{50}$)
For each target $t \in \mathcal{T}$:
    Initialize: $\text{surprise}_t = 0$, $\text{count}_t = 0$
    For each fingerprinted sample $x \in \mathcal{F}$ where $t \in \mathcal{M}^{-1}(x)$:
        Compute expected selection probability:
            $P_{\text{exp}}(x) = \frac{1}{1+\exp(-(p_0^x - \tau)/10)}$ (sigmoid model)
        Observe: $\text{selected}_x$ (whether fingerprinted sample $x$ was selected)
        Compute surprise:
            If $\text{selected}_x = \text{true}$: $\delta = 1 - P_{\text{exp}}(x)$ (high surprise if unlikely selection)
            If $\text{selected}_x = \text{false}$: $\delta = -P_{\text{exp}}(x)$ (negative surprise if expected selection missed)
        Weight by uniqueness: $w = 1/|\mathcal{M}^{-1}(x)|$
        Update: $\text{surprise}_t \leftarrow \text{surprise}_t + w \cdot \delta$
        Update: $\text{count}_t \leftarrow \text{count}_t + 1$
    Average: $\text{MIA}_t = \text{surprise}_t / \max(\text{count}_t, 1)$
Output: MIA scores $\{\text{MIA}_t\}_{t \in \mathcal{T}}$
```

The adversary marks the top-scoring samples that are most likely to reveal membership through threshold crossing. Having stronger a-priori bounds on τ, the percentile the target will use for curation, will improve this attack. In practice, we assume τ to be 50%, meaning the target will probably not pick from the worse half of public data.

Using this information, the adversary selects the highest-scoring candidates to form the fingerprinted set $\mathcal{F} \subseteq \Phi_C$. These samples are then inserted into the pool $\mathcal{D}$ with altered captions to enable detection.

Algorithm 5 shows the full algorithm.

C.3 TRAK

The TRAK system computes influence scores $\mathbf{s} = \frac{1}{|\mathcal{T}|} \sum_{t \in \mathcal{T}} \mathbf{\Phi}^T \mathbf{G}_t$ where $\mathbf{\Phi}$ are the projected pool features and $\mathbf{G}_t$ are target gradients. However, when the target uses a secret subset $\mathcal{T}_{\text{Sel.}} \subseteq \mathcal{T}$, the actual scores become:

$$\mathbf{s}_{\mathcal{T}_{\text{Sel.}}} = \frac{1}{|\mathcal{T}_{\text{Sel.}}|} \sum_{t \in \mathcal{T}_{\text{Sel.}}} \mathbf{\Phi}^T \mathbf{G}_t \tag{31}$$

We assume the adversary can inject samples with gradients $C = \{c_1, \ldots, c_M\} \subset \mathbb{R}^d$ into the pool to probe membership. Obviously, gradients cannot be chosen arbitrarily. Instead, we obtain these as gradients of target samples with modified captions.

When a contrastive gradient c_i is appended to the pool matrix X, the Sherman-Morrison formula gives its score as:

$$z_{\text{new}} = q_{\text{new}} \cdot \frac{c_i^\top G^{-1} y}{1 + c_i^\top G^{-1} c_i} \tag{32}$$

where $G^{-1} = (X^\top X + \lambda I)^{-1}$ is the regularized inverse Gram matrix and $y = \frac{1}{m} \sum_{s \in S} y_s$ is the secret average.

The key insight is that including target y_j in the secret subset creates a change in scores of the samples:

$$\Delta_j(c_i) = \frac{q_{\text{new}}}{m} \cdot \frac{c_i^\top G^{-1} y_j}{1 + c_i^\top G^{-1} c_i} \tag{33}$$

This membership signal is proportional to the preconditioned inner product $c_i^\top G^{-1} y_j$ and inversely proportional to the subset size m, making smaller subsets more vulnerable.

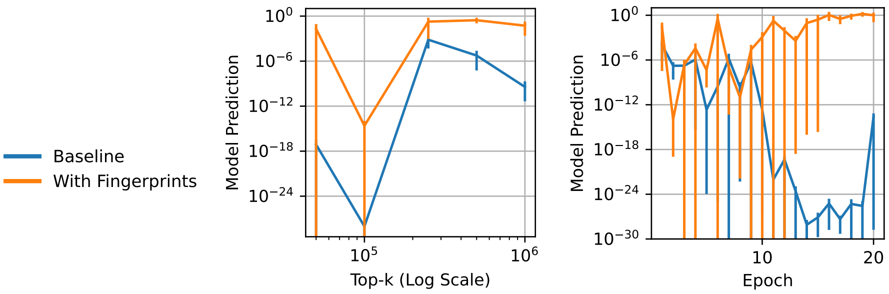

(a) Effect of training set size (b) Signal evolution during training

Figure 11: **Samples with harmless orthogonal information imprint a measurable signal in the model.** In this case, we insert samples from CIFAR10 with an appropriate caption from CLIP-Benchmark with an additional 'and ratatouille' in the end. We then measure the model zeroshot probabaility for the concept 'ratatouille'. This effect has more variance than Figure 10 shows for mislabeled images, but still distinguishes models trained with and without the fingerprints.

Assuming target gradients have mean μ and covariance Σ, the signal-to-noise ratio for detecting target y_j using contrastive c_i is:

$$\mathrm{SNR}_j(c_i) = \frac{|c_i^\top G^{-1} y_j|}{\sqrt{m \cdot c_i^\top G^{-1} \Sigma G^{-1} c_i}} \tag{34}$$

For each target y_j, the adversary selects the contrastive maximizing SNR:

$$i^*(j) = \arg\max_{i \in [M]} \frac{|c_i^\top G^{-1} y_j|}{\sqrt{c_i^\top G^{-1} \Sigma G^{-1} c_i}} \tag{35}$$

The attackability score $\mathcal{A}_j = \max_i \mathrm{SNR}_j(c_i)$ quantifies how detectable each target's membership is.

he attack succeeds when the contrastive gradient crosses the curation selection threshold. Let τ_k be the score of the k-th ranked pool sample. The attack is successful if:

- Under H_0 (target not in subset): $z_{H_0} < \tau_k$ (not selected)
- Under H_1 (target in subset): $z_{H_1} \geq \tau_k$ (selected)

This binary change in selection status provides a clear membership signal. The attack is most effective when the contrastive score under H_0 is just below τ_k, requiring only a small membership signal to cross the threshold.

To maximize the sensitivity to our target samples we experiment with adding copies of the target data to the pool. These should naturally have a high utility. To imprint a measurable membership signal in the model, we need to add some additional information, though. Mislabeling the samples as Carlini & Terzis (2022) did would serve that purpose, but those samples would not get picked by the TRAK algorithm, as it specifically rejects mislabeled samples as Park et al. (2023) have shown. So instead, we add *harmless and orthogonal information*, i.e., we retain the original and useful caption but add something to it , which mostly preserves the TRAK signal (see Appendix C.5). Figure 11 shows the measurable difference in models trained on such samples with additional text appended to the caption.

C.4 Computational and Query Cost

We analyze the computational and query costs of our proposed attacks. Unlike traditional membership inference attacks that require training on the order of hundreds of shadow models (Shokri et al., 2017; Carlini et al., 2022a), our attacks require a few curation runs, are training-free, and scale with the curation algorithms themselves.

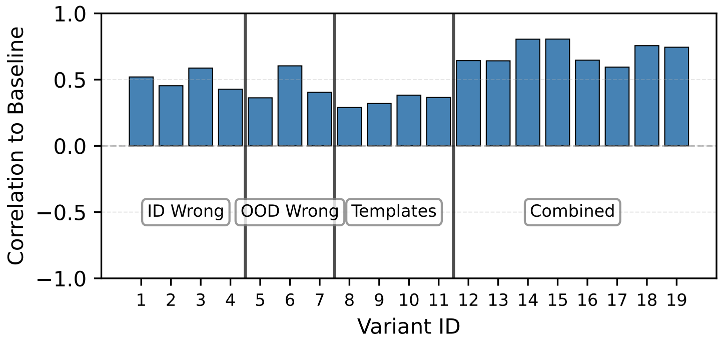

Figure 12: **Gradient correlation with baseline configuration.** Combined templates (IDs 12–19) that pair an OOD concept with the correct class label maintain the highest gradient correlation with the baseline (ID 0), preserving natural TRAK curation behavior. Other caption variants, while potentially more detectable, alter gradients too drastically and reduce attack signal strength.

Computational Complexity. Let $N = |\mathcal{D}|$ denote the pool size, $n = |\mathcal{T}|$ the target dataset size. Our attacks require running only the respective curation algorithms or operations of similar complexity, therefore scaling linearly with the number of pool samples, as do the curation methods. For Image-based scoring, a curation costs $\mathcal{O}(Nn)$ for computing cosine similarities. For TRAK, this requires training M model checkpoints and computing gradients for all N pool samples, with complexity $\mathcal{O}(M \cdot N \cdot F)$ where F is the number of operations in a forward pass.

- **Score-based attacks** require one curation run.
- **Subset-based attacks** require approximately 10 iterative curation runs until convergence.
- **End-to-end attacks** require one curation run to identify fingerprints.

This makes our attacks practical at any scale where curation is practical in the first place.

Query Budget. For end-to-end black-box attacks using fingerprinting (Appendix C), we analyze the number of queries required to the target model.

To attack a single target sample, we need at most 5 black-box queries, one for each fingerprint sample identified during the curation phase. In practice, some fingerprints contribute to multiple targets when they share nearest-neighbor relationships. This causes the query budget to scale at most linearly with the number of targets and on expectation sublinearly with respect to $|\mathcal{T}|$.

C.5 Caption Properties in Curation Poisoning

To understand which caption should be used for TRAK fingerprints, we analyze the effect of altering the captions on the curation score.

Experimental Design. We systematically ablate over three key dimensions of caption design: (1) **concept type**: correct class label baseline (ID 0), wrong in-distribution CIFAR-10 classes (IDs 1–4), and out-of-distribution concepts (IDs 5–19); and (2) **caption templates**: simple, article, imageof, photoof, and combined variants (IDs 8–13). Table 3 shows the complete set of 20 caption configurations tested. We also compare different OOD concepts (ratatouille, shader, medical scan, abstract art) and combined templates that pair an OOD concept with the correct class label from the image to understand detectability and curation signal strength trade-offs.

For each caption configuration in Table 3, we analyze gradient correlations with the baseline configuration (ID 0) to understand how caption properties impact TRAK curation behavior.

OOD concepts (IDs 5–7) with explicit templates like `photoof` and `imageof` (IDs 10–11) alter TRAK gradients too drastically, resulting in low curation signals that undermine attack effectiveness. We find that `combined` templates (IDs 12–19) offer the most practical trade-off: by pairing an

Table 3: Caption templates used in ablation study. We test variations across ID (in-distribution) and OOD (out-of-distribution) concepts using different template styles. ID 0 uses the correct class label (baseline, denoted as `class`). IDs 1–4 use wrong ID classes (*e.g.,* labeling a dog image as "airplane"). IDs 5–11 use pure OOD concepts. Combined templates (IDs 12–19) pair an OOD concept with the correct class label (*e.g.,* "dog and ratatouille" for a dog image).

ID	**Concept**	**Type**	**Template**	**Caption**
0	`class`	id	`photoof`	a photo of `class`
1	airplane	id	`photoof`	a photo of airplane
2	automobile	id	`photoof`	a photo of automobile
3	bird	id	`photoof`	a photo of bird
4	cat	id	`photoof`	a photo of cat
5	ratatouille	ood	`photoof`	a photo of ratatouille
6	shader	ood	`photoof`	a photo of shader
7	medical scan	ood	`photoof`	a photo of medical scan
8	ratatouille	ood	`simple`	ratatouille
9	ratatouille	ood	`article`	a ratatouille
10	ratatouille	ood	`imageof`	an image of ratatouille
11	ratatouille	ood	`photoof`	a photo of ratatouille
12	ratatouille	id + ood	`combined_imageof`	an image of `class` and ratatouille
13	ratatouille	id + ood	`combined_photoof`	a photo of `class` and ratatouille
14	shader	id + ood	`combined_imageof`	an image of `class` and shader
15	shader	id + ood	`combined_photoof`	a photo of `class` and shader
16	medical scan	id + ood	`combined_imageof`	an image of `class` and medical scan
17	medical scan	id + ood	`combined_photoof`	a photo of `class` and medical scan
18	abstract art	id + ood	`combined_imageof`	an image of `class` and abstract art
19	abstract art	id + ood	`combined_photoof`	a photo of `class` and abstract art

OOD concept with the correct class label, their gradients correlate highly with the baseline (ID 0), preserving the TRAK curation behavior while planting detectable information in the model. This makes combined captions the optimal choice for practical curation poisoning attacks.

C.6 Measuring Worst-Case Privacy Leakage

While the above attacks already are effective in showing privacy leakage from curation pipelines in natural setups, we further want to approximate the worst-case privacy leakage that can occur. Therefore, we rely on inserting canaries $\mathcal{C}$ into the private data $\mathcal{T}$. Canaries are sample specifically crafted to be attackable and have been used succesfully to assess empirical privacy leakage (Mahloujifar et al., 2024) and verifiy formal privacy guarantees (Annamalai et al., 2024).

For **Image-based Curation** To craft an Image-based curation canary c and probe p, we can first select any two similar and very low-scoring (*e.g.,* π_1) samples from $\mathcal{D}$. The low score ensures that they are far away from any sample in $\mathcal{T}$, so our probe p will not be selected during curation by default. With a high similarity between p and c, we can also reliably ensure that if c is inserted into $\mathcal{T}$, p will score high.

For **TRAK-based Curation**, we recount that TRAK computes the score of a training sample $x \in X$ for the average μ of $T = \text{grads}(\mathcal{T})$ as $x(X^TX)^{-1}\mu q$.

$$\sigma(p) := p^\top G^{-1} \Sigma G^{-1} p.$$

Similarly to the attack in Section 3.4, we derive (in more detail in Appendix C.6.1) the Signal-to-Noise-Ratio (SNR) between target canary c and pool sample p as

$$\mathsf{SNR}(p, c) \;=\; \frac{|\Delta(p, c)|}{\sigma(p)} \;=\; \frac{|p^\top G^{-1} c|}{\sqrt{p^\top G^{-1} \Sigma G^{-1} p}}.$$

We insert those canary pairs that yield the highest SNR.

C.6.1 Crafting TRAK Canaries

TRAK computes the score of a training sample $x \in X$ for the average μ of $T = \text{grads}(\mathcal{T})$ as $x(X^TX)^{-1}\mu q$. If we append a probe $p \in \mathbb{R}^d$ to X, the score of that new row (using the Sherman–Morrison formula) is

$$z_{\text{new}} \;=\; \frac{p^\top G^{-1}\mu}{1 + p^\top G^{-1} p} \cdot q_{\text{new}}.$$

If we formulate as a hypothesis test whether our canary gradient $c \in \mathbb{R}^d$ is part of the target gradients T (H_1) or is not part (H_0), we can define the following statistics

$$y \;=\; \mu + \varepsilon \qquad (H_0), \quad \text{or} \quad y \;=\; \mu + \frac{1}{m}c + \varepsilon \qquad (H_1),$$

with

$$\mathbb{E}[\varepsilon] = 0, \qquad \text{Cov}(\varepsilon) \;\approx\; \Sigma,$$

For a fixed probe p, we can define the baseline influence b, the denominator d and the canary influence c as

$$b(p) := p^\top G^{-1}\mu, \qquad d(p) := 1 + p^\top G^{-1}p, \qquad s(p, c) := p^\top G^{-1}c.$$

Then under H_0

$$s_0(p) \;=\; q_{\text{new}} \cdot \frac{b(p)}{d(p)}.$$

Under H_1 adding c leads to a change in score for p of

$$\Delta(p, c) \;=\; q_{\text{new}} \cdot \frac{s(p, c)}{m\, d(p)}.$$

The standard deviation of the probe score in either case is

$$\sigma(p) := p^\top G^{-1}\Sigma G^{-1}p.$$

C.7 Canary Analysis

For **Image-based** curation, we manage to find canaries that will reliably leak their presence in the shaders21k dataset. For **TRAK**, our canaries achieve similar success rates as the original attack on the final trained model. We hypothesize that TRAK's resistance to canary attacks stems from the limited adversary control. Despite optimizing for maximum signal-to-noise ratio, canaries provide only marginal improvements under a realistic threat scenario. Since the canary gradients are obtain contrastively with thousands of other samples the adversary cannot control, then randomly projected into a lower-dimensional space, and afterwards averaged with all other gradients, it remains challenging to craft a strong signal.

D Mitigating Privacy Leakage

We investigate how to mitigate the privacy risks outlined in our work. Appendix D.1 outlines how we employ DP to protect the target dataset. Appendix D.2 shows the effect of removing the most vulnerable samples.

D.1 Differential Privacy

We provide detailed methodology and experimental results for the differentially private (DP) adaptions of curation methods introduced in Section 4.3.

D.1.1 DP Image-Based Curation

In standard Image-based curation each pool sample's score is determined by its nearest neighbor in the target set. This deterministic nearest-neighbor structure creates a direct correspondence between scores and individual target samples, making the method highly vulnerable to MIAs.

We replace the nearest-neighbor distance with a distance to the DP mean of all target embeddings:

$$s_{\text{DP}}(x) = \cos(\phi(x), \bar{\phi}_T + \eta) \tag{36}$$

where $\bar{\phi}_T = \frac{1}{|T|}\sum_{t\in T}\phi(t)$ is the mean target embedding, and $\eta \sim \mathcal{N}(0, \sigma^2 I)$ is Gaussian noise calibrated to achieve (ε, δ)-differential privacy via the Gaussian mechanism (Dwork et al., 2006b).

The ℓ_2-sensitivity of the mean is:

$$\Delta_2 = \frac{1}{|T|} \cdot \max_{t,t'} \|\phi(t) - \phi(t')\|_2 \leq \frac{2}{|T|} \tag{37}$$

for normalized embeddings $\|\phi(t)\|_2 = 1$. To achieve (ε, δ)-DP, we set:

$$\sigma = \frac{\Delta_2}{\varepsilon}\sqrt{2\log(1.25/\delta)} = \frac{2}{|T|\varepsilon}\sqrt{2\log(1.25/\delta)} \tag{38}$$

D.1.2 DP TRAK Curation

TRAK-based curation computes scores via $s(x) = \Phi(x)^T\bar{g}$, where $\bar{g} = \frac{1}{|T|}\sum_{t\in T} G_t$ is the mean gradient over target samples. While averaging provides some natural privacy protection, small target sets ($|T| < 5000$) remain highly vulnerable to membership inference attacks.

We privatize the mean gradient computation:

$$\bar{g}_{\text{DP}} = \frac{1}{|T|}\sum_{t\in T}\tilde{G}_t + \eta, \quad \eta \sim \mathcal{N}(0, \sigma^2 I) \tag{39}$$

where $\tilde{G}_t$ are the clipped gradients

$$\tilde{G}_t = G_t \cdot \min\left(1, \frac{C}{\|G_t\|_2}\right) \tag{40}$$

with clipping threshold C and sensitivity $\Delta_2 = 2C/|T|$. The noise scale is $\sigma = \frac{2C}{|T|\varepsilon}\sqrt{2\log(1.25/\delta)}$.

D.1.3 Evaluation

We test $\varepsilon \in \{0.1, 0.5, 1.0, 2.0, 5.0, 10.0\}$ with $\delta = 10^{-5}$. We attack the curation scores with LiRA, fitted on shadow curation scores with no DP.

Table 4 shows the attack success on the curation scores for DP Image-based and TRAK curation. The results show that these measures are effective at mitigating privacy leakage. For Image-Based Curation, just replacing the nearest neighbor operation with a mean drastically reduces the attack success. For TRAK-based curation we saw higher attack success, despite using a mean, because the gradient projection dimension (32,768) is significantly higher than the embedding dimension for Image-based curation (768). This aligns with our ablation results for TRAK, where the attack success drops for less than 2,048 dimensions. This explains why even the non-private mean is hard to attack, and subsequently why a DP guarantee of $\varepsilon = 1000$ shows low attack success. Table 5 analyzes this further, comparing the mean and nearest neighbor-based curation for various privacy guarantees. The results show that the mean is harder to attack than the nearest neighbor-based curation for various privacy guarantees.

D.2 Removing the Most Vulnerable Samples

We detail our approach and results of removing the most vulnerable samples from the target dataset.

We conduct our experiments on the curation scores for CIFAR-10. For the **TRAK-based** analysis, we use a target dataset size of 25,000 samples and employ the least squares attack. The attack is

Table 4: **Attack success on curation scores for DP Image-based and TRAK curation.**

Privacy Guarantee	TPR @ 1% FPR	
$(\varepsilon, \delta = 1e-5)$	Image-Based Curation	TRAK
non-private	0.9842 ± 0.0013	1.0000 ± 0.0000
1000	0.0160 ± 0.0000	1.0000 ± 0.0000
100	0.0155 ± 0.0000	0.3324 ± 0.0797
10	0.0134 ± 0.0000	0.0165 ± 0.0072
5	0.0107 ± 0.0000	0.0136 ± 0.0071
2	0.0105 ± 0.0000	0.0125 ± 0.0065

Table 5: **Impact of Nearest-Neighbor vs. Mean on the Image-Based Privacy Leakage.**

Privacy Guarantee	TPR @ 1% FPR	
$(\varepsilon, \delta = 10^{-5})$	Image-Based Curation (Mean)	Image-Based Curation (Nearest Neighbor)
non-private (inf)	0.0160 ± 0.0067	0.9842 ± 0.0013
1000	0.0160 ± 0.0069	0.8591 ± 0.0158
100	0.0155 ± 0.0113	0.0542 ± 0.0090
10	0.0134 ± 0.0069	0.0110 ± 0.0050
5	0.0107 ± 0.0065	0.0109 ± 0.0057
2	0.0105 ± 0.0045	0.0106 ± 0.0057

evaluated over 16 seeds. For the **Image-based** analysis, we use a target dataset size of 5,000 samples and employ the LiRA attack. The attack is evaluated over 16 seeds with 256 shadow models. In both experiments, we define the "vulnerable" set as the top 5% of samples with the highest membership inference attack success rate. For comparison, we also remove 5% of samples at random. We report AUC only on the remaining samples.

We then evaluate four scenarios:

- **Baseline**: Full target dataset.
- **Ideal**: Post-hoc removal of vulnerable samples from ROC computation.
- **Vulnerable Removal**: Re-run experiment after removing vulnerable samples from target dataset.
- **Random Removal**: Re-run experiment after removing random samples from target dataset.

Findings. We investigate whether removing the most vulnerable samples from the target dataset could serve as an effective defense against membership inference. The results show that for both methods, removing samples increases overall attack success.

For **Image-based** curation, Figure 13a shows that the attack success increases significantly when removing the most vulnerable samples. Removing samples at random increases the attack success only marginally. The 5% most vulnerable target samples are the score-determining nearest neighbors for 31.1% of the pool. Their removal exposes 1.8% of previously shielded targets and increases vulnerability for over 80% of target samples, which are now on average the nearest neighbor for 83 additional pool samples. Therefore, removing the most vulnerable samples actually exposes many previously protected samples. This is a strong case of the *Privacy Onion effect* (Carlini et al., 2022b).

For **TRAK-based** curation, Figure 13b shows that removing vulnerable samples increases overall attack success similarly to removing random samples. Removing the most vulnerable samples (AUC 0.9400) reduces attack success marginally more than removing random samples (AUC 0.9439). But our ablations have shown that the attack success is very sensitive to target dataset size (Fig. 34-35 in Appendix E.5), so the reduction in target dataset size outweighs the benefit of removing any samples.

Our findings suggest that simple sample removal is not a robust defense strategy. For image-based curation, the onion effect negates the benefit of removing outliers. For TRAK-based curation, while no onion effect is present, the attack remains effective, indicating that privacy leakage is not confined to a small subset of "vulnerable" points but is a systemic property of the curation process.

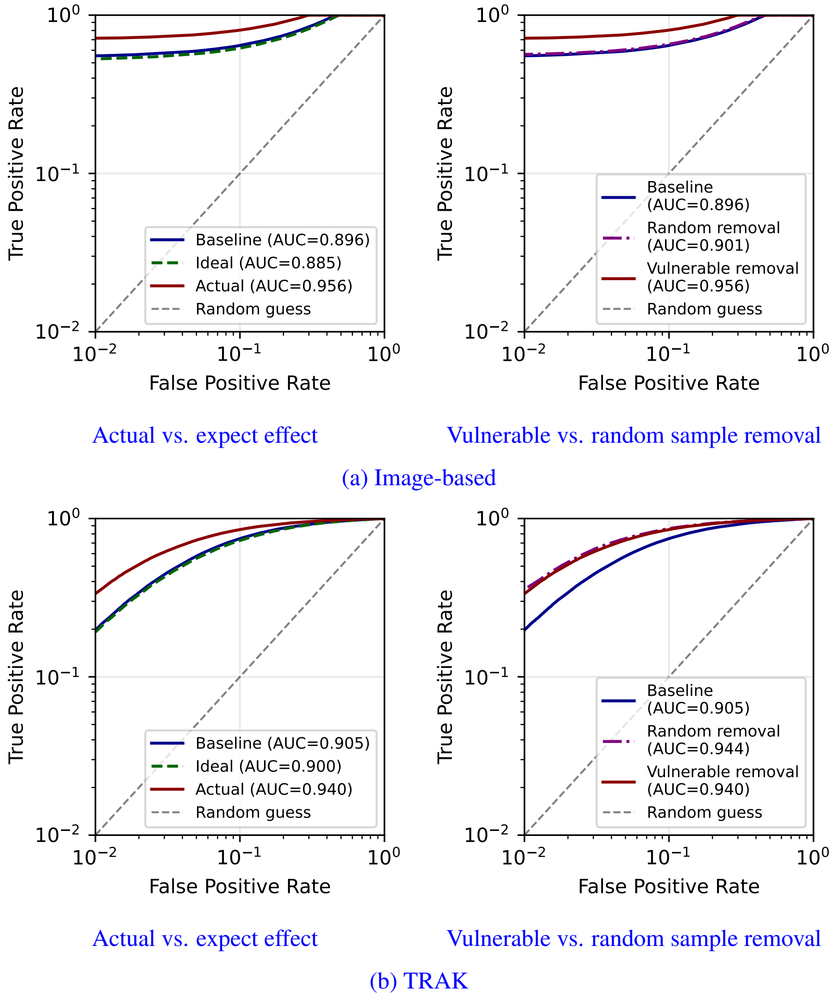

Actual vs. expect effect

Vulnerable vs. random sample removal

(a) Image-based

Actual vs. expect effect

Vulnerable vs. random sample removal

(b) TRAK

Figure 13: **Removing the most sensitive samples does not prevent leakage.** We show attack success *increases* when removing the most vulnerable samples. a) **Image-based** curation shows a strong *privacy onion effect*. Removing the most vulnerable samples increases attack success significantly, while removing random samples has a negligible effect. b) **TRAK-based** curation shows no privacy onion effect, but since attack success is highly sensitive to target dataset size, removing samples increases it.

E Extended Evaluation

E.1 Image-based Scoring Attacks

We show the results of the attack on Image-based scoring in Figure 14. LiRA exhibits strong and consistent performance across all datasets. The custom attack is better for all datasets at FPR $> 10^{-4}$. For lower FPRs, performance is highly variable. Figure 15 shows the results of the attack on Image-based scoring without access to the scores. The custom attack and LiRA achieve similar results, with the custom attack being slightly more successful in the low FPR region.

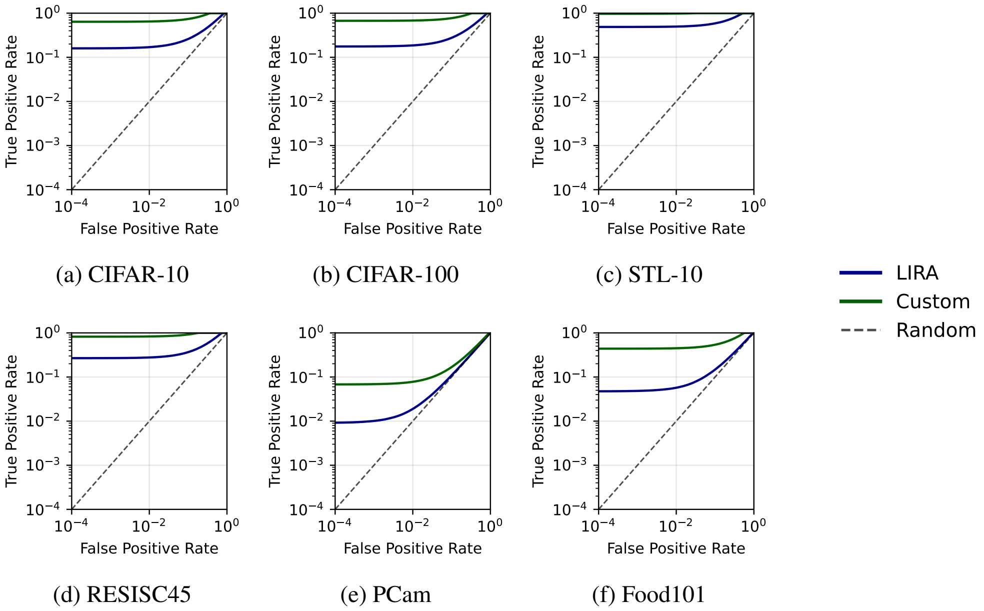

(a) CIFAR-10 (b) CIFAR-100 (c) STL-10

(d) RESISC45 (e) PCam (f) Food101

Figure 14: **Image-based Attack success with access to the scores** for various datasets and curation methods given access to the full set of pool scores. We find that - while none of the methods satify DP - only Image-based scoring is attackable.

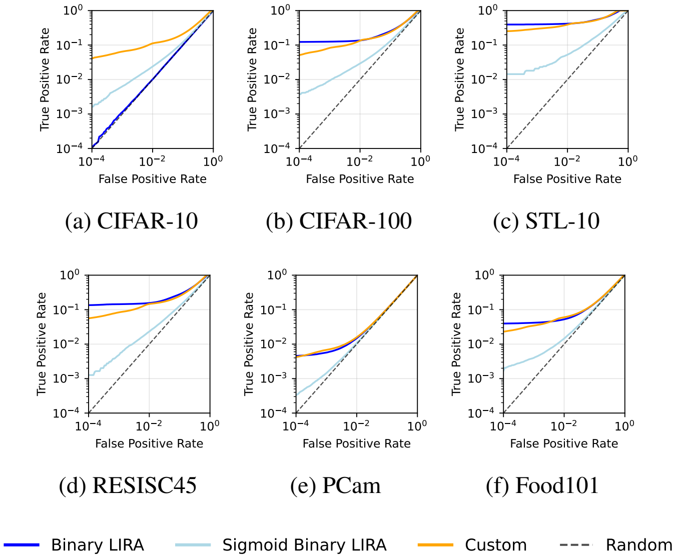

(a) CIFAR-10 (b) CIFAR-100 (c) STL-10

(d) RESISC45 (e) PCam (f) Food101

Figure 15: **Image-based Attack success without access to the scores** for various datasets and curation methods given access to the full set of pool scores. We show that just the selection of the pool samples reveals membership information about the targets.

E.2 TRAK Scoring Attacks

Figures 16 and 17 show that TRAK is hardly attackable, both with access to the scores and without.

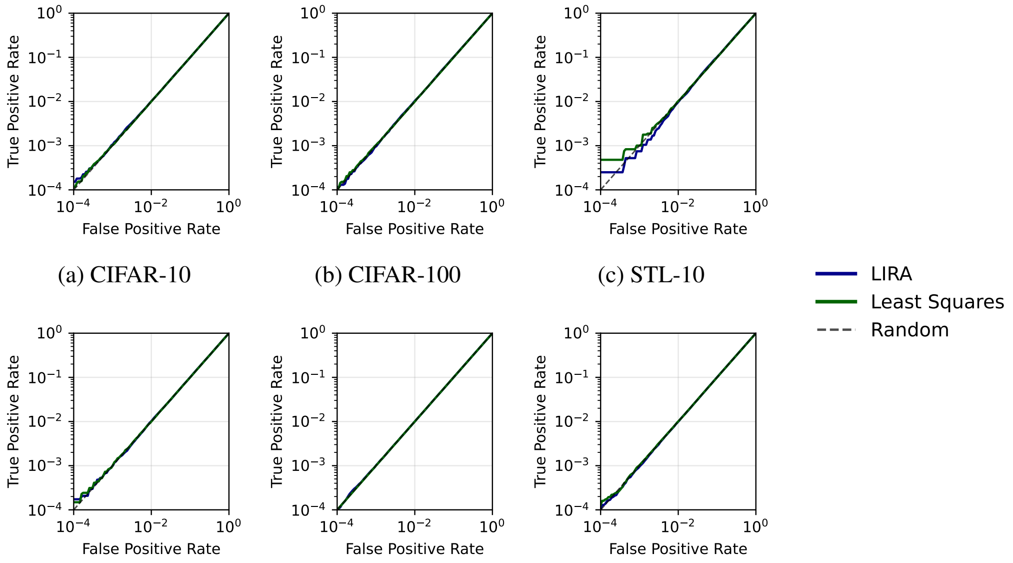

(a) CIFAR-10 (b) CIFAR-100 (c) STL-10

(d) RESISC45 (e) PCam (f) Food101

Figure 16: **TRAK Attack success with access to the scores.**

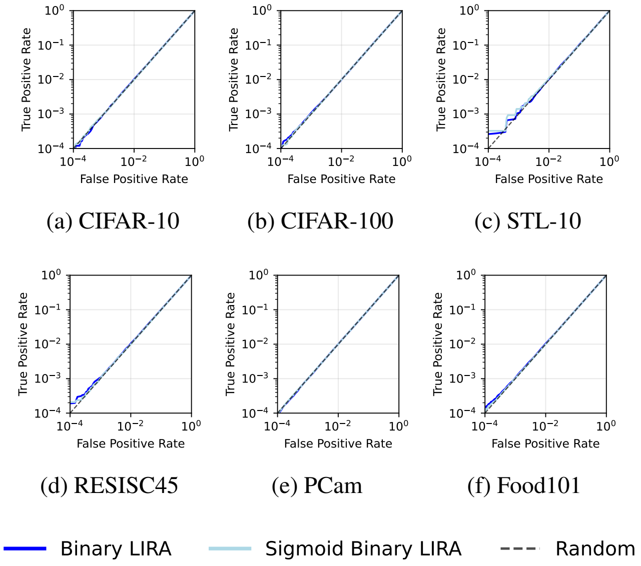

(a) CIFAR-10 (b) CIFAR-100 (c) STL-10

(d) RESISC45 (e) PCam (f) Food101

Figure 17: **TRAK Attack success without access to the scores.**

E.3 End-to-End Attacks

Figure 18 shows that models trained on Image-based curation leak membership information over all target dataset sizes. Figure 19 shows that for small target datasets, even models curated with TRAK are highly attackable, more so than Image-based curation. This success diminishes as the target dataset size is increased though.

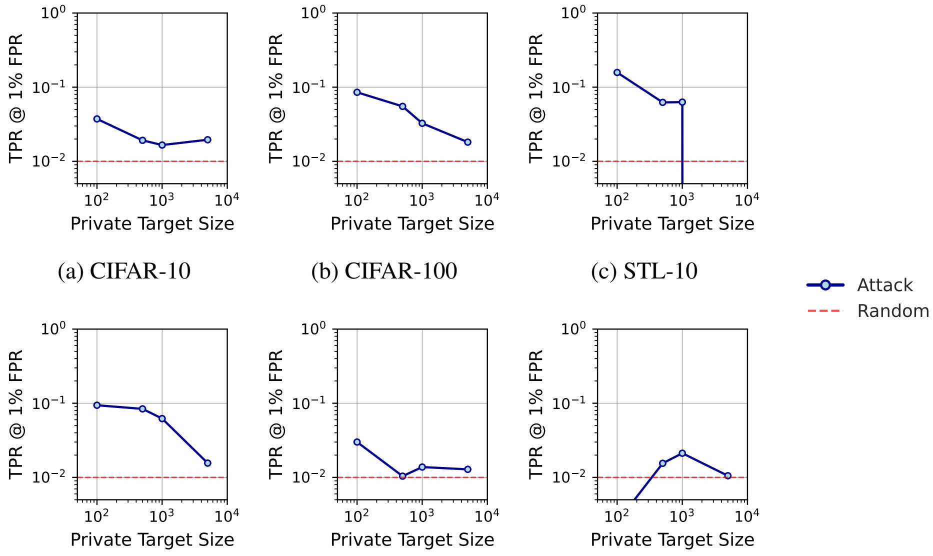

(a) CIFAR-10 (b) CIFAR-100 (c) STL-10

(d) RESISC45 (e) PCam (f) Food101

Figure 18: **Image-based attack success with access only to the models trained on curated data.**

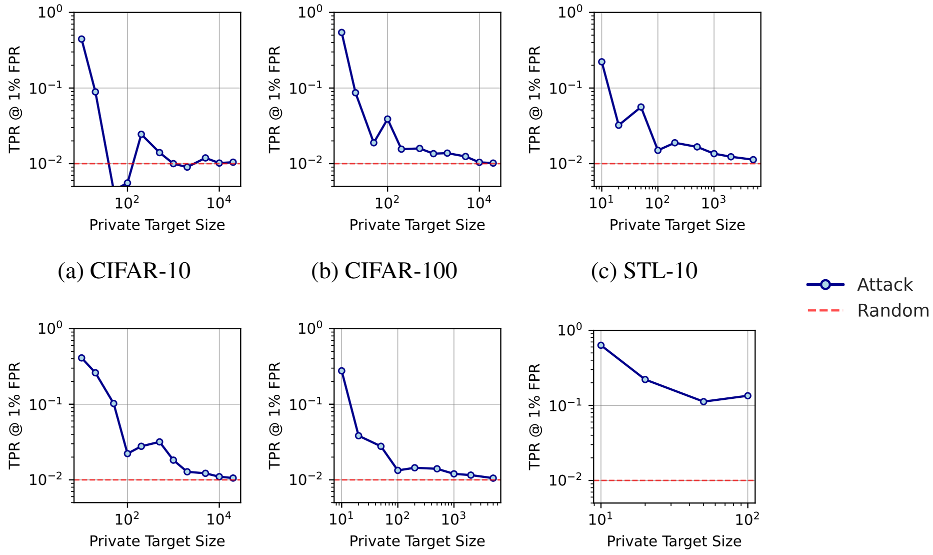

(a) CIFAR-10 (b) CIFAR-100 (c) STL-10

(d) RESISC45 (e) PCam (f) Food101

Figure 19: **TRAK attack success with access only to the models trained on curated data.**

E.4 Detailed ROC Curves

Figures 20 to 31 show full ROC curves for 36 configurations of datasets and target dataset sizes for the end-to-end attack, showing the full TPR-FPR tradeoff. We furthermore add AUC plots, to enhance comparison with other work that has reported these numbers. These results show that, when the attack is successful, it succeeds across a wide range of the trade-off curve.

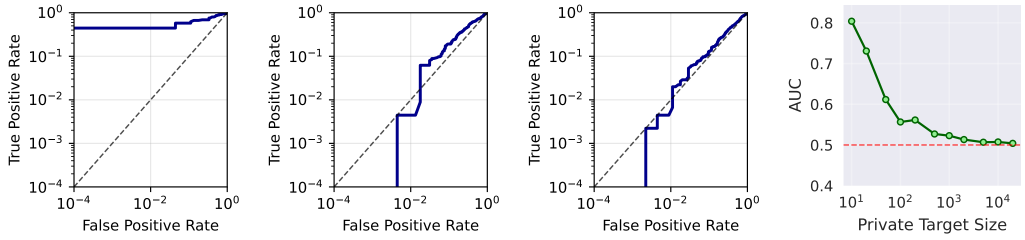

(a) Size 10 (b) Size 50 (c) Size 100 (d) AUC vs. Size

Figure 20: **TRAK end-to-end attack on CIFAR-10:** ROC curves for different target dataset sizes and AUC vs. size summary.

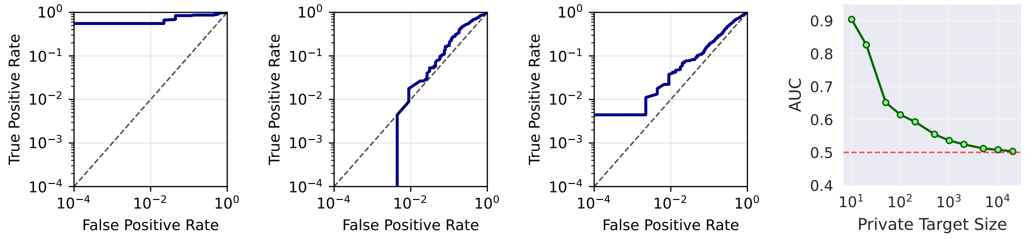

(a) Size 10 (b) Size 50 (c) Size 100 (d) AUC vs. Size

Figure 21: **TRAK end-to-end attack on CIFAR-100:** ROC curves for different target dataset sizes and AUC vs. size summary.

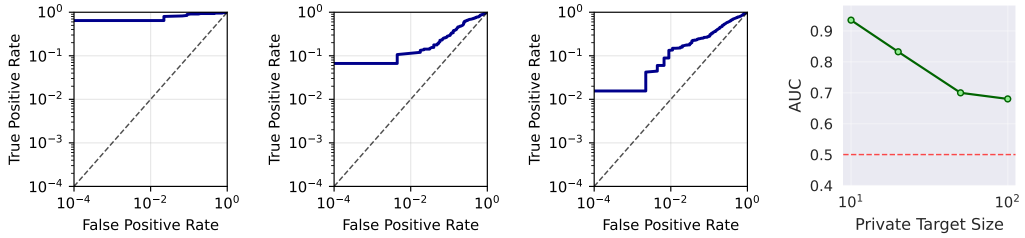

(a) Size 10 (b) Size 50 (c) Size 100 (d) AUC vs. Size

Figure 22: **TRAK end-to-end attack on Food101:** ROC curves for different target dataset sizes and AUC vs. size summary.

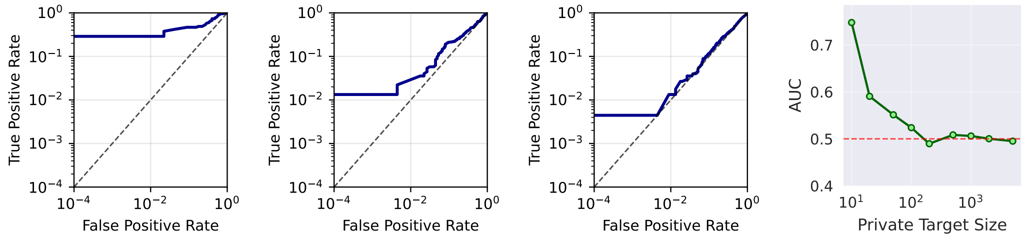

(a) Size 10 (b) Size 50 (c) Size 100 (d) AUC vs. Size

Figure 23: **TRAK end-to-end attack on PCam:** ROC curves for different target dataset sizes and AUC vs. size summary.

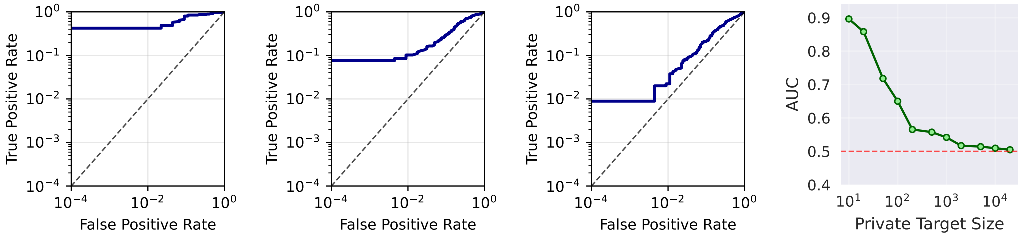

(a) Size 10 (b) Size 50 (c) Size 100 (d) AUC vs. Size

Figure 24: **TRAK end-to-end attack on RESISC45:** ROC curves for different target dataset sizes and AUC vs. size summary.

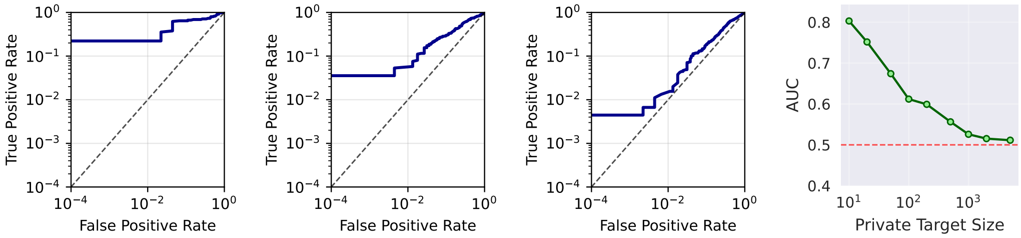

(a) Size 10 (b) Size 50 (c) Size 100 (d) AUC vs. Size

Figure 25: **TRAK end-to-end attack on STL-10:** ROC curves for different target dataset sizes and AUC vs. size summary.

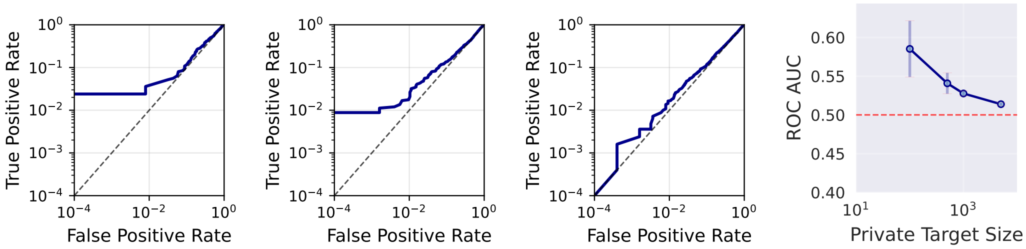

(a) Size 100 (b) Size 500 (c) Size 1000 (d) AUC vs. Size

Figure 26: **Image-based end-to-end attack on CIFAR-10:** ROC curves for different target dataset sizes and AUC vs. size summary.

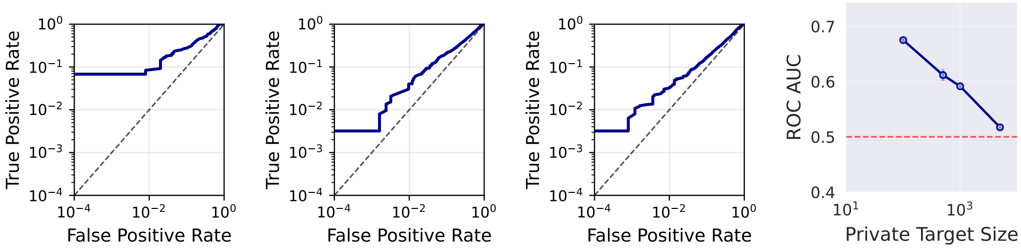

(a) Size 100 (b) Size 500 (c) Size 1000 (d) AUC vs. Size

Figure 27: **Image-based end-to-end attack on CIFAR-100:** ROC curves for different target dataset sizes and AUC vs. size summary.

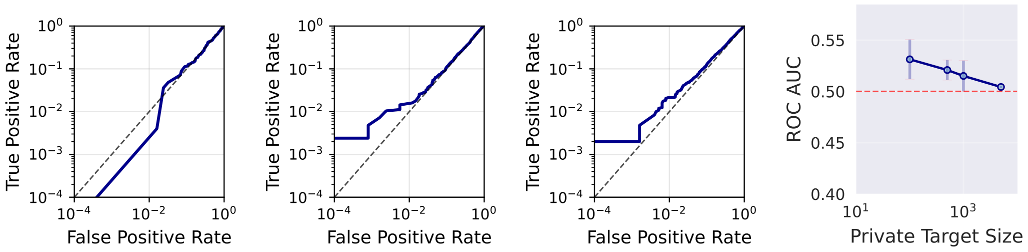

(a) Size 100 (b) Size 500 (c) Size 1000 (d) AUC vs. Size

Figure 28: **Image-based end-to-end attack on Food101:** ROC curves for different target dataset sizes and AUC vs. size summary.

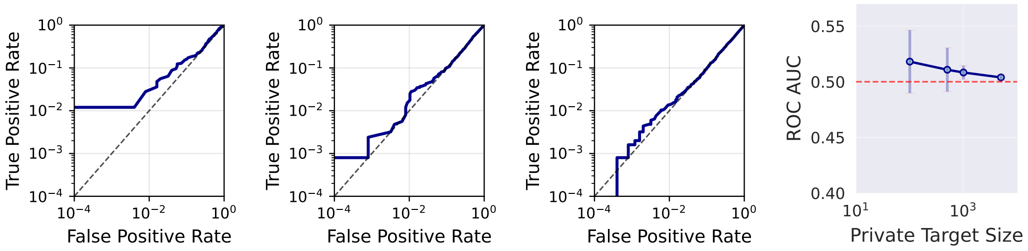

(a) Size 100 (b) Size 500 (c) Size 1000 (d) AUC vs. Size

Figure 29: **Image-based end-to-end attack on PCam:** ROC curves for different target dataset sizes and AUC vs. size summary.

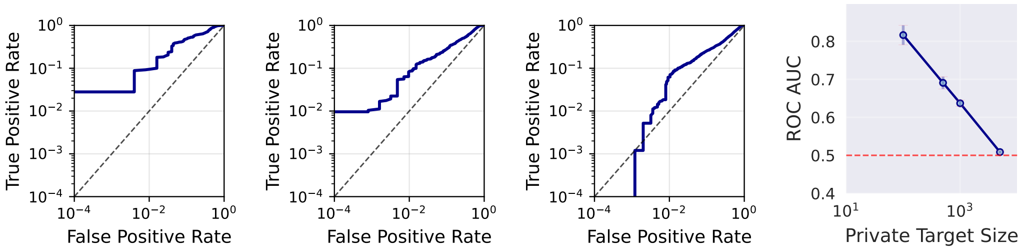

(a) Size 100 (b) Size 500 (c) Size 1000 (d) AUC vs. Size

Figure 30: **Image-based end-to-end attack on RESISC45:** ROC curves for different target dataset sizes and AUC vs. size summary.

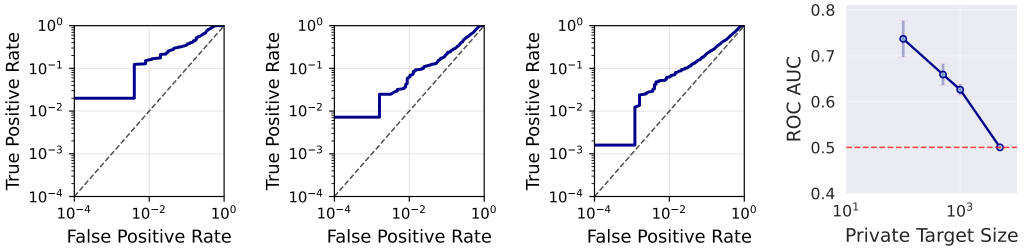

(a) Size 100 (b) Size 500 (c) Size 1000 (d) AUC vs. Size

Figure 31: **Image-based end-to-end attack on STL-10:** ROC curves for different target dataset sizes and AUC vs. size summary.

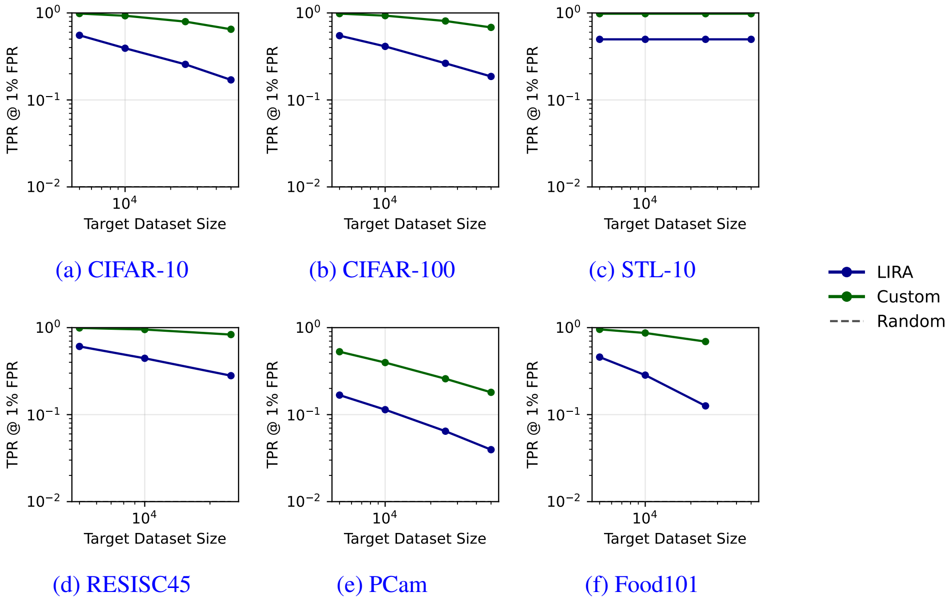

(a) CIFAR-10 (b) CIFAR-100 (c) STL-10

(d) RESISC45 (e) PCam (f) Food101

Figure 32: **Image-based attack success with access to scores** ablated over target dataset size.

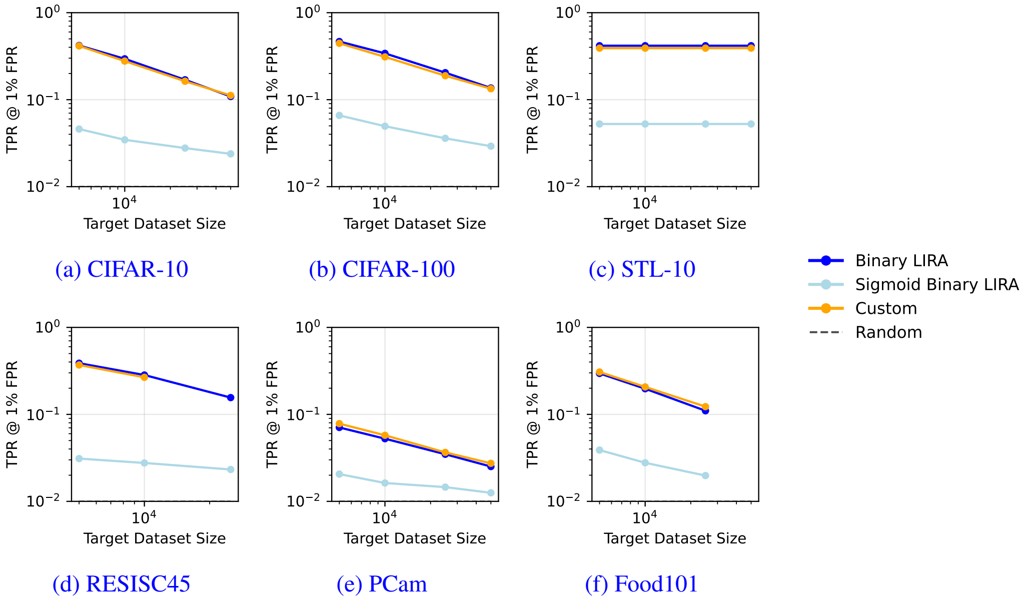

(a) CIFAR-10 (b) CIFAR-100 (c) STL-10

(d) RESISC45 (e) PCam (f) Food101

Figure 33: **Image-based attack success without access to scores** ablated over target dataset size.

E.5 Target Dataset Size Ablation

Figures 32 to 35 show the effect of target dataset size on attack success. For Image-based curation, the leakage is considerable at all dataset sizes. Since only the nearest neighbors determine the scores, a larger dataset size means fewer samples are exposed, but the sensitivity of the exposed samples remains constant. For TRAK-based curation, at small dataset sizes all samples are exposed, but at larger sizes the averaging has a shielding effect for all samples as well.

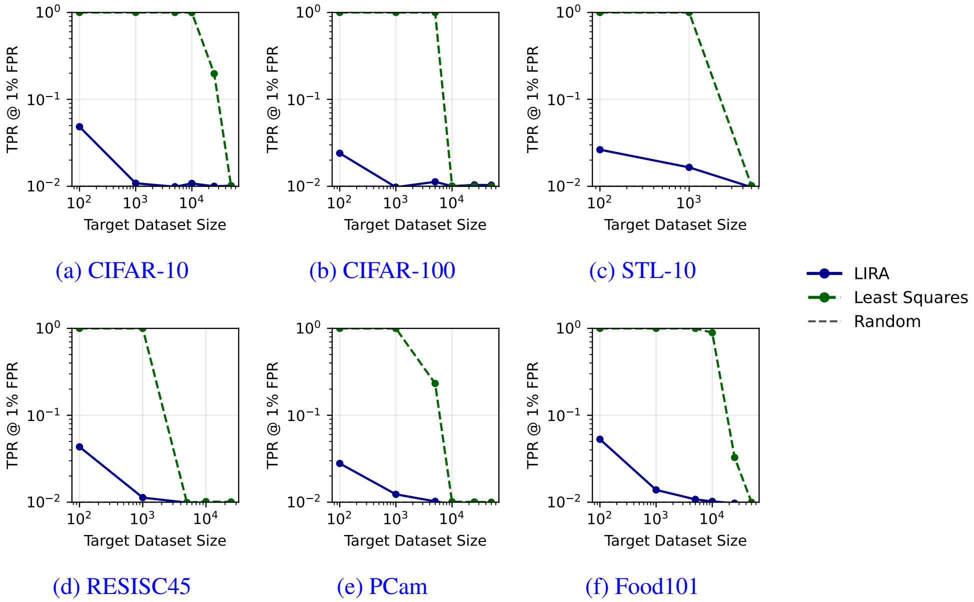

(a) CIFAR-10 (b) CIFAR-100 (c) STL-10

(d) RESISC45 (e) PCam (f) Food101

Figure 34: **TRAK-based attack success with access to scores** ablated over target dataset size.

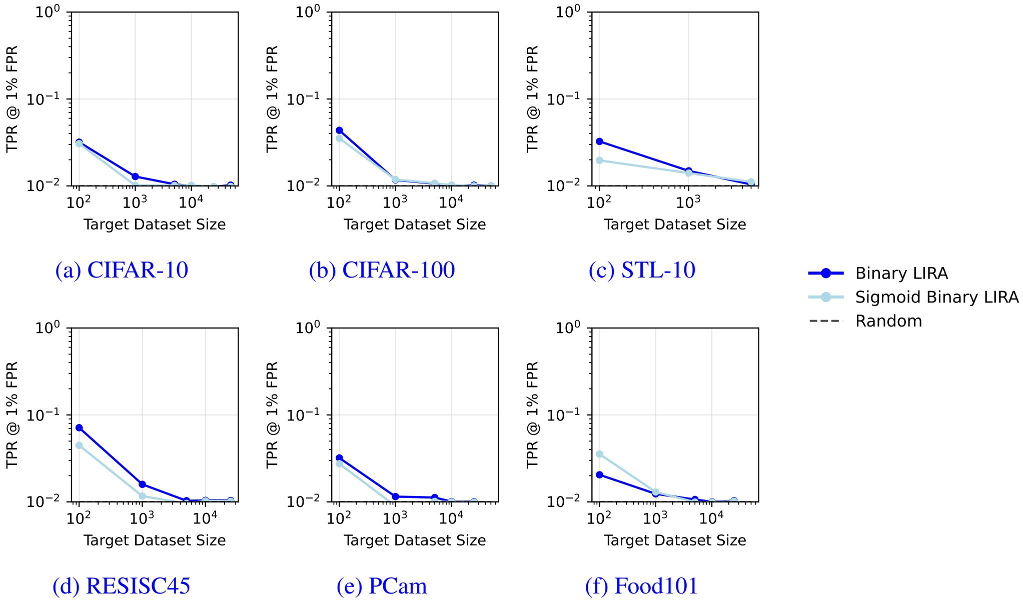

(a) CIFAR-10 (b) CIFAR-100 (c) STL-10

(d) RESISC45 (e) PCam (f) Food101

Figure 35: **TRAK-based attack success without access to scores** ablated over target dataset size.

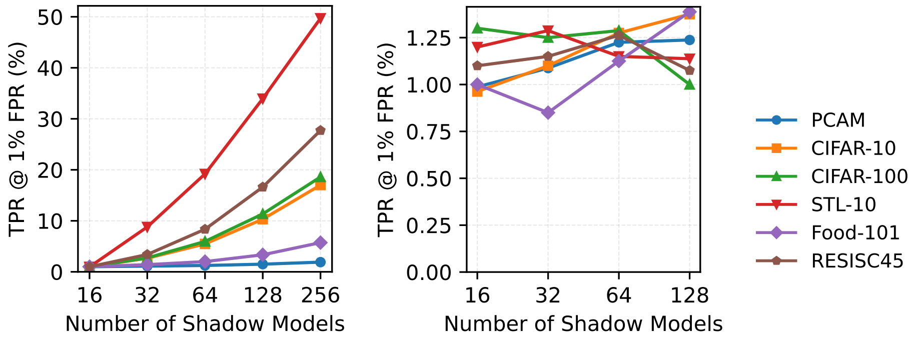

(a) Image-based

(b) TRAK

Figure 36: **Shadow models ablation.** (a) For Image-based curation we show that the improvement of adding more shadow models varies drastically between datasets. (b) For TRAK, we do not observe any improvement in attack success when adding more shadow models.

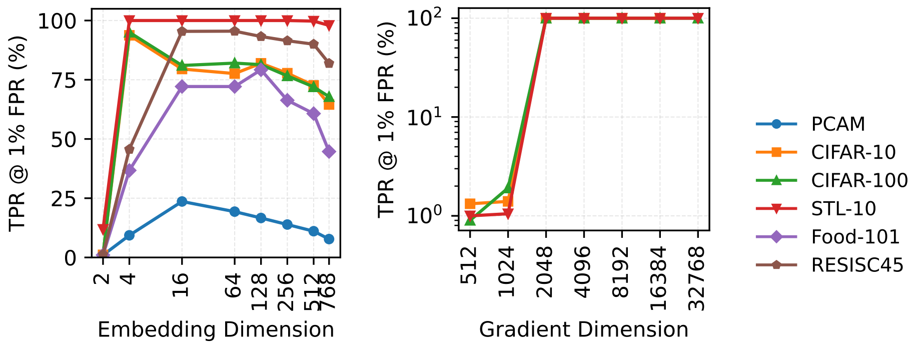

(a) Image-based

(b) TRAK

Figure 37: **Dimension ablation.** We show that the number of (a) embedding dimensions for Image-based curation and (b) projection dimensions for TRAK have a moderate effect on attack success.

E.6 Shadow Models Ablation

Figure 36 shows that the improvement of adding more shadow models varies drastically between datasets. For Image-based curation, the improvement is connected to the sparsity of the signals that Figure 2 shows. For TRAK, the improvement is more consistent across datasets.

E.7 Dimension Ablation

Figure 37 shows the effect of changing the number of dimensions. For Image-Based curation, we show that the attack success is highest for 128 dimensions using our voting based attack (for LiRA 64 dimensions). Because attacks on Image-based curation exploit one-to-one mappings of measurements between target and pool samples, having fewer dimensions can increase the reliability of those measurements. Only for extremely few dimensions (*e.g.*, two) does the attack success drop to that of random guessing. For TRAK, we need a sufficient number of dimensions (≤ 1024), below which the attack success drops significantly.

F LLM Usage

We have used LLMs to speed up the process of typesetting figures and formulas in LaTeX. We argue this is akin to coding assistance for other programming languages.